Pair of accelerated black holes in an anti–de Sitter background: The AdS *C* metric

Óscar J. C. Dias* and José P. S. Lemos†
Centro Multidisciplinar de Astrofísica–CENTRA, Departamento de Física, Instituto Superior Técnico, Av. Rovisco Pais 1, 1049-001 Lisboa, Portugal

(Received 7 October 2002; published 10 March 2003)

The anti–de Sitter *C* metric (AdS *C* metric) is characterized by a quite interesting new feature when compared with the *C* metric in flat or de Sitter backgrounds. Indeed, contrary to what happens in these two last exact solutions, the AdS *C* metric only describes a pair of accelerated black holes if the acceleration parameter satisfies $A>1/\ell$, where ℓ is the cosmological length. The two black holes cannot interact gravitationally and their acceleration is totally provided by the pressure exerted by a strut that pushes the black holes apart. Our analysis is based on the study of the causal structure, on the description of the solution in the AdS 4-hyperboloid in a 5D Minkowski spacetime, and on the physics of the strut. We also analyze the cases $A=1/\ell$ and $A<1/\ell$ that represent a single accelerated black hole in the AdS background.

DOI: 10.1103/PhysRevD.67.064001 PACS number(s): 04.20.Jb, 04.20.Gz, 04.70.Bw

I. INTRODUCTION

The original *C* metric was found by Levi-Civita in his studies between 1917 and 1919. During the following decades, many authors rediscovered it and studied its mathematical properties (see [1] for references). In 1963, Ehlers and Kundt [2] classified degenerated static vacuum fields and put this Levi-Civita solution into the *C* slot of the table they constructed. From then onwards this solution has been called the *C* metric. This spacetime is stationary, axially symmetric, Petrov type D, and is an exact solution which includes a radiative term. Although the *C* metric had been studied from a mathematical point of view along the years, its physical interpretation remained unknown until 1970, when Kinnersley and Walker [3], in a groundbreaking work, showed that the solution describes two uniformly accelerated black holes in opposite directions. Indeed, they noticed that the original solution was geodesically incomplete, and by defining new suitable coordinates they analytically extended it and studied its causal structure. The solution has a conical singularity in one of its angular poles that was interpreted by them as due to the presence of a strut in between pushing the black holes away, or as two strings from infinity pulling in each one of the black holes. The strut or the strings lie along the symmetry axis and cause the acceleration of the black hole pair. This work also included for the first time the charged version of the *C* metric. In an important development, Ernst in 1976 [4], through the employment of an appropriate transformation, removed all the conical singularities of the charged *C* metric by appending an external electromagnetic field. In this new exact Ernst solution, the acceleration of the pair of oppositely charged black holes is provided by the Lorentz force associated with the external field. The geometric properties of the *C* metric were further investigated by Farhoosh and Zimmerman [5], and the asymptotic properties of the *C* metric were analyzed by Ashtekar and Dray [6], who showed that null infinity admits a conformal completion, has a spherical section, and moreover that the causal diagrams drawn in [3] were not quite accurate. The issue of physical interpretation of the *C* metric was recovered by Bonnor [7], but now following a different approach. He transformed the *C* metric into the Weyl form in which the solution represents a finite line source (that corresponds to the horizon of the black hole), a semi-infinite line mass (corresponding to a horizon associated with uniform accelerated motion), and a strut keeping the line sources apart. By applying a further transformation that enlarges this solution, Bonnor confirmed the physical interpretation given in [3]. Bonnor's procedure was simplified by Cornish and Uttley and extended to include the massive charged solution [8]. More recently, Yongcheng [9], starting from the metric of two superposed Schwarzschild black holes, derived the *C* metric under appropriate conditions. The black hole uniqueness theorem for the *C* metric was proven by Wells [10] and the geodesic structure of the *C* metric was studied by Pravda and Pravdova [11]. The limit at which the acceleration goes to infinity was analyzed by Podolský and Griffiths [12], who showed that in this limit the solution is analogous to the one which describes a spherical impulsive gravitational wave generated by a snapping string. We note that the *C* metric is an important and explicit example of a general class of asymptotically flat radiative spacetimes with boost-rotation symmetry and with hypersurface orthogonal axial and boost Killing vectors. The geometric properties of this general class of spacetimes were investigated by Bičák and Schmidt [13] and the radiative features were analyzed by Bičák [14] (see the recent review of Pravda and Pravdova [15] on this class of spacetimes and the role of the *C* metric).

Relevant generalizations to the *C* metric were made by Plebański and Demiański in 1976 [16] and by Dowker, Gauntlett, Kastor, and Traschen in 1994 [17]. Plebański and Demiański, in addition to the mass (m) and electromagnetic charge (q), have included into the solution a Newman-Unti-Tamburino (NUT) parameter, a rotation, and a cosmological constant term (Λ), and Dowker *et al.* have further included a dilaton field nonminimally coupled. Thus, the most general *C* metric has eight parameters so far, namely acceleration, mass, electric and magnetic charges, NUT parameter, rota-

*Electronic address: oscar@fisica.ist.utl.pt
†Electronic address: lemos@kelvin.ist.utl.pt

tion, cosmological constant, and dilaton field. The C metric with mass and electromagnetic charges alone was extensively studied as shown above, and from now on we will refer to it as the flat C metric (i.e., C metric with $\Lambda=0$). The C metric with a NUT parameter has not been studied, as far as we know. The flat spinning C metric was studied by Farhoosh and Zimmerman [18], Letelier and Oliveira [19], and by Bičák and Pravda [20]. In particular, in [20] the flat spinning C metric was transformed into the Weyl form and interpreted as two uniformly accelerated spinning black holes connected by a strut. This solution constitutes an example of a spacetime with axial and boost Killing vectors which are not hypersurface-orthogonal. Dowker *et al.* generalized the flat C metric and flat Ernst solution to include a dilaton field and applied these solutions for the first time in the context of quantum pair creation of black holes that once created, accelerate apart.

In what concerns the cosmological C metric introduced in [16], the de Sitter (dS) case ($\Lambda>0$) was analyzed by Podolský and Griffiths [21], whereas the anti–de Sitter (AdS) case ($\Lambda<0$) was studied, in special instances, by Emparan, Horowitz, and Myers [22] and by Podolský [23]. In general, the C metric (either flat, dS or AdS) describes a pair of accelerated black holes. Indeed, in the flat and dS backgrounds this is always the case. However, in an AdS background the situation is not so simple and depends on the relation between the acceleration A of the black holes and the cosmological length ℓ. Since the AdS C metric presents such peculiar features, it deserves a careful analysis. It is our intention in this paper to fully study, in its most general form, the AdS C metric with mass, charge, and cosmological constant. One can divide the study into three cases, namely $A<1/\ell$, $A=1/\ell$ and $A>1/\ell$. The $A<1/\ell$ case was the one analyzed by Podolský [23], and the $A=1/\ell$ case was investigated by Emparan, Horowitz, and Myers [22], which has acquired an important role since the authors showed that, in the context of a lower dimensional Randall-Sundrum model, it describes the final state of gravitational collapse on the brane-world. The geodesic structure of this solution has been studied by Chamblin [24]. Both cases, $A<1/\ell$ and $A=1/\ell$, represent one single accelerated black hole. The case $A>1/\ell$ has not been fully studied and its physical interpretation is not yet firmly established, although it has been applied, in addition to the flat and dS cases, in pair creation of black holes by Hawking, Horowitz, and Ross [25] and by Mann [26] (see [27] for a review). The purpose of this paper is to establish that the $A>1/\ell$ AdS C metric describes a pair of accelerated black holes in an AdS background. This aim will be achieved through a thorough analysis of the causal structure of the solution, together with the description of the solution in the AdS 4-hyperboloid, and the study of the strut's physics.

The plan of this paper is as follows. In Sec. II, we present the AdS C metric and analyze its curvature and conical singularities. In Sec. III, we study the causal diagrams of the solution. In Sec. IV, we give and justify a physical interpretation to the solution. The description of the solution in the AdS 4-hyperboloid and the physics of the strut are analyzed. These two sections, Secs. III and IV, are highly related, and so, in order to fully understand both of them, the reading of each is required. Finally, in Sec. V concluding remarks are presented.

II. GENERAL PROPERTIES OF THE AdS C METRIC

A. The AdS C metric

The AdS C metric, i.e., the C metric with negative cosmological constant Λ, was obtained by Plebański and Demiański [16]. For zero rotation and zero NUT parameter it is given, according to [16] (see also [26]), by

$$ds^2=1/(\tilde{x}+\tilde{y})^2(-\mathcal{F}d\tilde{t}^2+\mathcal{F}^{-1}d\tilde{y}^2+\mathcal{G}^{-1}d\tilde{x}^2+\mathcal{G}d\tilde{z}^2), \tag{1}$$

where

$$\mathcal{F}(\tilde{y})=-\Lambda/6-\tilde{A}^2+\tilde{y}^2-2m\tilde{y}^3+q^2\tilde{y}^4,$$
$$\mathcal{G}(\tilde{x})=-\Lambda/6+\tilde{A}^2-\tilde{x}^2-2m\tilde{x}^3-q^2\tilde{x}^4. \tag{2}$$

The meaning of parameters $\tilde{A}$, m, and q will be clarified soon. For the benefit of comparison with the flat C metric, we note that when Λ vanishes we have $\mathcal{F}(\tilde{y})=-\mathcal{G}(-\tilde{y})$. It is now convenient to redefine the parameter $\tilde{A}$ as $-\Lambda/6+\tilde{A}^2\equiv A^2$, together with the coordinate transformations: $\tilde{t}=t/A$, $\tilde{y}=Ay$, $\tilde{x}=Ax$, and $\tilde{z}=z/A$. With these redefinitions, the gravitational field of the AdS C metric is written as

$$ds^2=[A(x+y)]^{-2}(-\mathcal{F}dt^2+\mathcal{F}^{-1}dy^2+\mathcal{G}^{-1}dx^2+\mathcal{G}dz^2), \tag{3}$$

where

$$\mathcal{F}(y)=\left(\frac{1}{\ell^2A^2}-1\right)+y^2-2mAy^3+q^2A^2y^4,$$
$$\mathcal{G}(x)=1-x^2-2mAx^3-q^2A^2x^4, \tag{4}$$

and the nonzero components of the electromagnetic vector potential, $A_\mu dx^\mu$, are given by

$$A_t=-ey, \quad A_z=gx. \tag{5}$$

This solution depends on the following four parameters: A, which is the acceleration of the black hole; m, which is interpreted as the Arnowitt-Deser-Misner (ADM) mass of the nonaccelerated black hole; q, which is interpreted as the ADM electromagnetic charge of the nonaccelerated black hole and, in general, $q^2=e^2+g^2$, with e and g being the electric and magnetic charges, respectively; and finally the cosmological length $\ell^2\equiv 3/|\Lambda|$. The meaning attributed to the parameter A will be understood in Sec. IV, while the physical interpretation given to the parameters m and q is justified in the Appendix. We will consider the case $A>0$.

The coordinates used in Eqs. (3)–(5) to describe the AdS C metric are useful to understand the geometrical properties of the spacetime, but they hide the physical interpretation of

the solution. In order to understand the physical properties of the source and gravitational field, we will introduce progressively new coordinates more suitable to this purpose, following the approach of Kinnersley and Walker [3] and Ashtekar and Dray [6]. Although the alternative approach of Bonnor simplifies the interpretation in a way, we cannot use it since the cosmological constant prevents such a coordinate transformation into the Weyl form.

B. Radial coordinate: Curvature singularities

We start by defining a coordinate r as

$$r=[A(x+y)]^{-1}. \tag{6}$$

In order to interpret this coordinate as being a radial coordinate, we calculate a curvature invariant of the metric, namely the Kretschmann scalar,

$$R_{\mu\nu\alpha\beta}R^{\mu\nu\alpha\beta}=\frac{24}{\ell^2}+\frac{8}{r^8}[6m^2r^2+12mq^2(2Axr-1)r + q^4(7-24Axr+24A^2x^2r^2)]. \tag{7}$$

Clearly, this curvature invariant is equal to $24/\ell^2$ when the mass m and charge q are both zero. When at least one of these parameters is not zero, the curvature invariant diverges at $r=0$, revealing the presence of a curvature singularity. Moreover, when we take the limit $r\to\infty$, the curvature singularity approaches the expected value for a spacetime which is asymptotically AdS. Therefore, it is justified that r is interpreted as a radial coordinate.

C. Angular surfaces: Conical singularities

To gain more insight into the physical nature of the AdS C metric we now turn our attention into the angular surfaces $t=$const and $r=$const, hereafter labeled by Σ. In this section, we follow [3]. In order to have the AdS C metric with correct signature $(-+++)$, one must restrict the coordinate x to a domain on which the function $\mathcal{G}(x)$ is nonnegative [see Eq. (3)]. The shape of this function depends crucially on the three parameters A, m, and q. In this work, we will select only the ranges of these three parameters for which $\mathcal{G}(x)$ has at least two real roots, x_s and x_n (say), and require that x belong to the range $[x_s,x_n]$, where $\mathcal{G}(x)\geqslant 0$. This restriction has the important advantage of allowing us to endow the angular surfaces Σ with the topology of a compact surface. In these surfaces, we now define two new coordinates,

$$\theta=\int_x^{x_n}\mathcal{G}^{-1/2}dx,$$

$$\phi=z/\kappa, \tag{8}$$

where ϕ ranges between $[0,2\pi]$ and κ is an arbitrary positive constant which will be needed later when regularity conditions at the poles are discussed. The coordinate θ ranges between the north pole, $\theta=\theta_n=0$, and the south pole, $\theta=\theta_s$ (not necessarily at π). With these transformations the metric restricted to the surfaces Σ, $d\sigma^2=r^2(\mathcal{G}^{-1}dx^2+\mathcal{G}dz^2)$, takes the form

$$d\sigma^2=r^2(d\theta^2+\kappa^2\mathcal{G}d\phi^2). \tag{9}$$

When $A=0$ or when both $m=0$ and $q=0$, Eq. (8) gives $x=\cos\theta$, $\mathcal{G}=1-x^2=\sin^2\theta$, and if we use the freedom to put $\kappa\equiv 1$, the metric restricted to Σ is given by $d\sigma^2=r^2$ $(d\theta^2+\sin^2\theta d\phi^2)$. This implies that in this case the angular surface is a sphere and justifies the label given to the new angular coordinates defined in Eq. (8). In this case, the north pole is at $\theta_n=0$ or $x_n=+1$ and the south pole is at $\theta_s=\pi$ or $x_s=-1$. In the other cases x and $\sqrt{\mathcal{G}}$ can always be expressed as elliptic functions of θ. The explicit form of these functions is of no need in this work. All we need to know is that these functions have a period given by $2\theta_s$.

As we shall see, the regularity analysis of the metric in the region $[0,\theta_s]$ will play an essential role in the physical interpretation of the AdS C metric. The function $\mathcal{G}$ is positive and bounded in $]0,\theta_s[$ and thus the metric is regular in this region between the poles. We must be more careful with the regularity analysis at the poles, i.e., at the roots of $\mathcal{G}$. Indeed, if we draw a small circle around the north pole, in general, as the radius goes to zero, the limit circumference/radius is not 2π. Therefore, in order to avoid a conical singularity at the north pole one must require that $\delta_n=0$, where

$$\delta_n\equiv 2\pi\left(1-\lim_{\theta\to 0}\frac{1}{\theta}\sqrt{\frac{g_{\phi\phi}}{g_{\theta\theta}}}\right)=2\pi\left(1-\frac{\kappa}{2}\left|\frac{d\mathcal{G}}{dx}\right|_{x_n}\right). \tag{10}$$

Repeating the procedure, this time for the south pole, x_s, we conclude that the conical singularity at this pole can also be avoided if

$$\delta_s\equiv 2\pi\left(1-\frac{\kappa}{2}\left|\frac{d\mathcal{G}}{dx}\right|_{x_s}\right)=0. \tag{11}$$

The as yet arbitrary parameter κ introduced in Eq. (8) plays an important role here. Indeed, if we choose

$$\kappa^{-1}=\frac{1}{2}\left|\frac{d\mathcal{G}}{dx}\right|_{x=x_s}, \tag{12}$$

Equation (11) is satisfied. However, since we only have a single constant κ at our disposal and this has been fixed to remove the conical singularity at the south pole, we conclude that the conical singularity will be present at the north pole. There is another alternative. We can choose instead $2\kappa^{-1}=|d_x\mathcal{G}|_{x=x_n}$ (where d_x means the derivative in order to x) and by doing so we avoid the deficit angle at the north pole and leave a conical singularity at the south pole. In Sec. IV, we will see that in the extended Kruskal solution the north pole points towards the other black hole, while the south pole points towards infinity. The first choice of κ corresponds to a strut between the black holes while the alternative choice corresponds to two strings from infinity into each black hole. We leave the discussion on the physical nature of the conical

singularities and on the two possible choices for the value of κ to Sec. IV A 4. There is a small number of very special cases for which the very particular condition $|d_x\mathcal{G}|_{x_n} = |d_x\mathcal{G}|_{x_s}$ is verified. In these special cases, the solution is free of conical singularities. They will be mentioned below.

Since we have managed to put $\mathcal{G}(x)$ in a form equal to [3], we can now, following [3] closely, describe the behavior of $\mathcal{G}(x)$ for different values of the parameters A, m, and q. We can divide this discussion into three cases.

(i) *Massless uncharged solution* ($m=0,\ q=0$). In this case, we have $x=\cos\theta$, $\mathcal{G}=1-x^2=\sin^2\theta$, and $\kappa=1$. The angular surface Σ is a sphere and this is a particular case for which both the north and south poles are free of conical singularities.

(ii) *Massive uncharged solution* ($m>0,\ q=0$). The massive uncharged case must be divided into $mA<3^{-3/2}$ and $mA\geqslant 3^{-3/2}$. When $mA<3^{-3/2}$, $\mathcal{G}(x)$ has three roots and, as justified above, we require x to lie between the two roots for which $\mathcal{G}(x)\geqslant 0$. In doing so, we maintain the metric with the correct signature and have an angular surface Σ which is compact. Setting the value of κ given in Eq. (12), one avoids the conical singularity at the south pole but leaves one at the north pole. When $mA\geqslant 3^{-3/2}$, Σ is an open angular surface. For this reason, hereafter we will analyze only the case $mA<3^{-3/2}$.

(iii) *Massive charged solution* ($m>0,\ q\neq 0$). For a general massive charged solution, depending on the values of the parameters A, m, and q, $\mathcal{G}(x)$ can be positive in a single compact interval, $]x_s,x_n[$, or in two distinct compact intervals, $]x_s',x_n'[$ and $]x_s,x_n[$, say. In this latter case, we will work only with the interval $[x_s,x_n]$ (say) for which the charged solutions reduce to the uncharged solutions when $q=0$. These solutions have a conical singularity at one of the poles. The only massive charged solutions that are totally free of conical singularities are those which satisfy the particular conditions $m=|q|$ and $mA>1/4$. This indicates that in this case the AdS C metric is an AdS black hole written in an accelerated coordinate frame. In the massless charged solution ($m=0$ and $q\neq 0$), $\mathcal{G}(x)$ is an even function, has two symmetric roots, and is positive between them. The angular surface Σ is therefore compact and there are no conical singularities at both poles. Once again, this suggests that the solution is written in an accelerated coordinate frame.

D. Coordinate ranges

In this section, we analyze the important issue of the coordinate ranges. Rewritten in terms of the new coordinates introduced in Eq. (6) and Eq. (8), the AdS C metric is given by

$$ds^2=r^2[-\mathcal{F}(y)dt^2+\mathcal{F}^{-1}(y)dy^2 + d\theta^2+\kappa^2\mathcal{G}(x_{(\theta)})d\phi^2], \tag{13}$$

where $\mathcal{F}(y)$ and $\mathcal{G}(x_{(\theta)})$ are given by Eq. (4). The time coordinate t can take any value from the interval $]-\infty,+\infty[$ and ϕ ranges between $[0,2\pi]$. As we saw in Sec. II B, when m or q are not zero, there is a curvature singularity at $r=0$. Therefore, we restrict the radial coordinate to the range $[0,+\infty[$. On the other hand, in Sec. II C we have decided to consider only the values of A, m, and q for which $\mathcal{G}(x)$ has at least two real roots, x_s and x_n (say), and we have required that x belong to the range $[x_s,x_n]$, where $\mathcal{G}(x)\geqslant 0$. By doing this, we guarantee that the metric has the correct signature $(-+++)$ and that the angular surfaces Σ ($t=$const and $r=$const) are compact. From $Ar=(x+y)^{-1}$ we then conclude that y must belong to the range $-x\leqslant y<+\infty$. Indeed, $y=-x$ corresponds to $r=+\infty$, and $y=+\infty$ to $r=0$. Note, however, that when both m and q vanish, there are no restrictions on the ranges of r and y (i.e., $-\infty<r<+\infty$ and $-\infty<y<+\infty$) since in this case there is no curvature singularity at the origin of r to justify the constraint on the coordinates.

III. CAUSAL STRUCTURE OF THE AdS C METRIC

In this section we analyze the causal structure of the solution. As occurs with the original flat C metric [3,6], the original AdS C metric, Eq. (13), is not geodesically complete. To obtain the maximal analytic spacetime, i.e., to draw the Carter-Penrose diagrams, we will introduce the usual null Kruskal coordinates.

We now look carefully to the AdS C metric, Eq. (13), with $\mathcal{F}(y)$ given by Eq. (4). We first notice that, contrary to what happens in the $\Lambda\geqslant 0$ background where the causal structure and physical nature of the corresponding C metric is independent of the relation between the acceleration A and $\ell\equiv\sqrt{3/|\Lambda|}$, in the $\Lambda<0$ case we must distinguish and analyze separately the cases $A>1/\ell$, $A=1/\ell$, and $A<1/\ell$. Later, in Sec. IV, we will justify physically the reason for this distinction. The mathematical reason for this difference is clearly identified by setting $m=0$ and $q=0$ in Eq. (4), giving $\mathcal{F}(y)=y^2-[1-1/(\ell^2A^2)]$. Since the horizons of the solution are basically given by the real roots of $\mathcal{F}(y)$, we conclude that we have to treat separately the cases (A) $A>1/\ell$, for which $\mathcal{F}(y)$ can have two real roots, (B) $A=1/\ell$, for which $y=0$ is a double root, and (C) $A<1/\ell$, for which $\mathcal{F}(y)$ has no real roots (see the discussion in the text of Fig. 1). We will consider each of these three cases separately in Secs. III A and IV A ($A>1/\ell$ case), III B and IV B ($A=1/\ell$ case), and III C and IV C ($A<1/\ell$ case). The description of the solution depends crucially on the values of m and q. In each subsection, we will consider the three most relevant solutions, namely (i) the massless uncharged solution ($m=0,\ q=0$), (ii) the massive uncharged solution ($m>0,\ q=0$), and (iii) the massive charged solution ($m>0,\ q\neq 0$).

A. Causal structure of the $A>1/\ell$ solutions

1. Massless uncharged solution ($m=0$, $q=0$)

In this case, we have

$$\mathcal{F}(y)=y^2-y_+^2 \quad \text{with} \quad y_+=\sqrt{1-\frac{1}{\ell^2A^2}}, \tag{14}$$

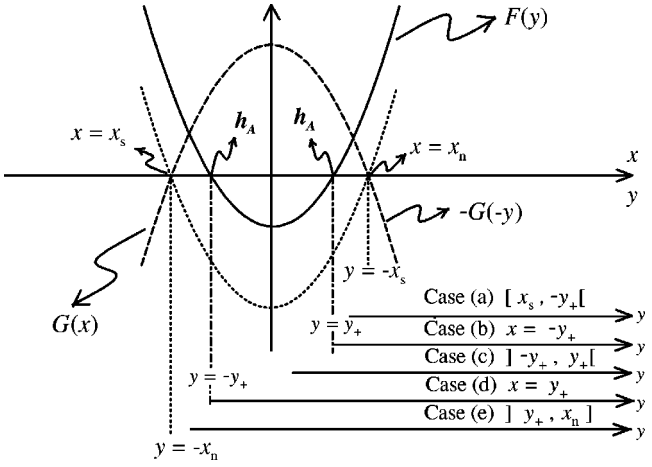

FIG. 1. Shape of $\mathcal{G}(x)$ and $\mathcal{F}(y)$ for the $A>1/\ell$, $m=0$, and $q=0$ C metric studied in Secs. III A 1 and IV A. The allowed range of x is between $x_s=-1$ and $x_n=+1$, where $\mathcal{G}(x)$ is positive and compact. The permitted range of y depends on the angular direction $x(-x\leqslant y<+\infty)$ and is sketched for the five cases (a)–(e) discussed in the text. The presence of an accelerated horizon is indicated by h_A. [For completeness, we comment here on two other cases not represented in the figure but analyzed in the text: for $A=1/\ell$, $m=0$, and $q=0$ (this case is studied in Secs. III B 1 and IV B), $\mathcal{F}(y)$ is zero at its minimum and positive elsewhere. For $A<1/\ell$, $m=0$, and $q=0$ (this case is studied in Secs. III C 1 and IV C), $\mathcal{F}(y)$ is always positive and only case (a) survives.]

and $x\in[x_s=-1,x_n=+1]$, $x=\cos\theta$, $\mathcal{G}=1-x^2=\sin^2\theta$, and $\kappa=1$. The shapes of $\mathcal{F}(y)$ and $\mathcal{G}(x)$ are represented in Fig. 1.

The angular surfaces Σ ($t=$const and $r=$const) are spheres and both the north and south poles are free of conical singularities. The origin of the radial coordinate, $r=0$, has no curvature singularity and therefore both r and y are in the range $]-\infty,+\infty[$. However, in the general case, where m or q are nonzero, there is a curvature singularity at $r=0$. Since the discussion of the present section is only a preliminary to that of the massive general case, following [6], we will treat the origin $r=0$ as if it had a curvature singularity and thus we admit that r belongs to the range $[0,+\infty[$ and y lies in the region $-x\leqslant y<+\infty$. We leave a discussion on the extension to negative values of r to Sec. IV A.

The general procedure to draw the Carter-Penrose diagrams is as follows. First, we make use of the null condition $g_{\mu\nu}k^\mu k^\nu=0$ (where k^μ is a geodesic tangent) to introduce the advanced and retarded Finkelstein-Eddington null coordinates,

$$u=t-y_*, \quad v=t+y_*, \tag{15}$$

where the tortoise coordinate is

$$y_*=\int \mathcal{F}^{-1}dy=\frac{1}{2y_+}\ln\left|\frac{y-y_+}{y+y_+}\right| \tag{16}$$

and both u and v belong to the range $]-\infty,+\infty[$. In these coordinates, the metric is given by

$$ds^2=r^2[-\mathcal{F}du\,dv+d\theta^2+\sin^2\theta d\phi^2]. \tag{17}$$

The metric still has coordinate singularities at the roots of $\mathcal{F}$. To overcome this unwanted feature, we have to introduce Kruskal coordinates. Now, due to the lower restriction on the value of y ($-x\leqslant y$), the choice of the Kruskal coordinates (and therefore the Carter-Penrose diagrams) depends on the angular direction x we are looking at. In fact, depending on the value of x, the region accessible to y might contain two, one, or zero roots of $\mathcal{F}$ (see Fig. 1) and so the solution may have two, one, or zero horizons, respectively. This angular dependence of the causal diagram is not new. The Schwarzschild and Reissner-Nordström solutions being spherically symmetric do not present this feature but, in the Kerr solution, the Carter-Penrose diagram along the pole direction is different from the diagram along the equatorial direction. Such a dependence occurs also in the flat C metric [3]. Back again to the AdS C metric, we have to consider separately five distinct sets of angular directions, namely (a) $x_s\leqslant x<-y_+$, (b) $x=-y_+$, (c) $-y_+<x<y_+$, (d) $x=+y_+$, and (e) $y_+<x\leqslant x_n$, where $x_s=-1$ and $x_n=+1$ (see Fig. 1).

(a) $x_s\leqslant x<-y_+$. Within this interval of the angular direction, the restriction on the range of y, $-x\leqslant y<+\infty$, implies that the function $\mathcal{F}(y)$ is always positive in the accessible region of y (see Fig. 1), and thus the solution has no horizons. Introducing the null coordinates defined in Eq. (15) followed by the Kruskal coordinates $u'=-e^{-y_+u}<0$ and $v'=+e^{+y_+v}>0$ gives $u'v'=-e^{2y_+y_*}=-(y-y_+)/(y+y_+)<0$, and Eq. (17) becomes

$$ds^2=r^2\left[-\frac{(y+y_+)^2}{y_+^2}du'dv'+d\theta^2+\sin^2\theta d\phi^2\right], \tag{18}$$

where y and $r=A^{-1}(x+y)^{-1}$ are regarded as functions of u' and v',

$$y=y_+\frac{1-u'v'}{1+u'v'}, \quad r=\frac{1}{A}\frac{1+u'v'}{(y_++x)-u'v'(y_+-x)}. \tag{19}$$

Now, let us find the values of the product $u'v'$ at $r=0$ and $r=+\infty$,

$$\lim_{r\to 0}u'v'=-1,$$

$$\lim_{r\to+\infty}u'v'=\frac{y_++x}{y_+-x}<0 \text{ and finite.} \tag{20}$$

So, for $x_s\leqslant x<-y_+$, the original massless uncharged AdS C metric is described by Eq. (18) subjected to the following coordinates ranges:

$$0\leqslant\phi<2\pi, \quad -1\leqslant x\leqslant+1, \quad u'<0, v'>0, \tag{21}$$

$$-1\leqslant u'v'<\frac{y_++x}{y_+-x}. \tag{22}$$

This spacetime is, however, geodesically incomplete. To obtain the maximal analytical extension, one allows the Kruskal coordinates to take also the values $u' \geqslant 0$ and $v' \leqslant 0$ as long as Eq. (22) is satisfied.

Finally, to construct the Carter-Penrose diagram one has to define the Carter-Penrose coordinates by the usual arctangent functions of u' and v'—$\mathcal{U} = \arctan u'$ and $\mathcal{V} = \arctan v'$—that bring the points at infinity into a finite position. In general, to find what kind of curve describes the lines $r=0$ or $r=+\infty$, one has to take the limit of $u'v'$ as $r \to 0$ (in the case of $r=0$) and the limit of $u'v'$ as $r \to +\infty$ (in the case of $r=+\infty$). If this limit is 0 or ∞, the corresponding line is mapped into a curved null line. If the limit is -1, or a negative and finite constant, the corresponding line is mapped into a curved timelike line and, finally, when the limit is $+1$, or a positive and finite constant, the line is mapped into a curved spacelike line. The asymptotic lines are drawn as straight lines, although in the coordinates $\mathcal{U}$ and $\mathcal{V}$ they should be curved outwards, i.e., bulged. It is always possible to change coordinates so that the asymptotic lines are indeed straight lines. So, from Eq. (20) we draw the Carter-Penrose diagram sketched in Fig. 2(a). There are no horizons and both $r=0$ and $r=+\infty$ ($\mathcal{I}$) are timelike lines.

(b) $x=-y_+$. For this particular angular direction, y is restricted to be on $+y_+ \leqslant y < +\infty$ and $\mathcal{F}(y)$ is always positive except at $y=+y_+$ (which corresponds to $r=+\infty$), where it is zero (see Fig. 1). Therefore, the solution has no horizon and the Kruskal construction is similar to the one described above in case (a). The only difference is that now $\lim_{r \to +\infty} u'v' = 0$ and thus $r=+\infty$ ($\mathcal{I}$) is represented by a null line in the Carter-Penrose diagram, which is shown in Fig. 2(b).

(c) $-y_+ < x < y_+$. The demand that y must belong to the range $[-x; +\infty[$ implies, for this range of the angular direction, that we have a region I, $-x \leqslant y < +y_+$, where $\mathcal{F}(y)$ is negative and a region II, $+y_+ < y < +\infty$, where $\mathcal{F}(y)$ is positive (see Fig. 1). There is a single Rindler-like acceleration horizon (r_A) at $y=+y_+$, so called because it is absent when $A=0$ and present even when $m=0$ and $q=0$. In region I, one sets the Kruskal coordinates $u' = +e^{-\alpha u}$ and $v' = +e^{+\alpha v}$ so that $u'v' = +e^{2\alpha y}*$. In region II, one defines $u' = -e^{-\alpha u}$ and $v' = +e^{+\alpha v}$ in order that $u'v' = -e^{2\alpha y}*$. We set $\alpha \equiv y_+$. Thus, in both regions the product $u'v'$ is given by

$$u'v' = -\frac{y-y_+}{y+y_+}, \tag{23}$$

and Eq. (17) expressed in terms of the Kruskal coordinates is given by

$$ds^2 = r^2 \left[\frac{1}{y_+^2} \frac{\mathcal{F}}{u'v'} du'dv' + d\theta^2 + \sin^2\theta \, d\phi^2 \right] \tag{24}$$

$$= r^2 \left[-\frac{(y+y_+)^2}{y_+^2} du'dv' + d\theta^2 + \sin^2\theta \, d\phi^2 \right]. \tag{25}$$

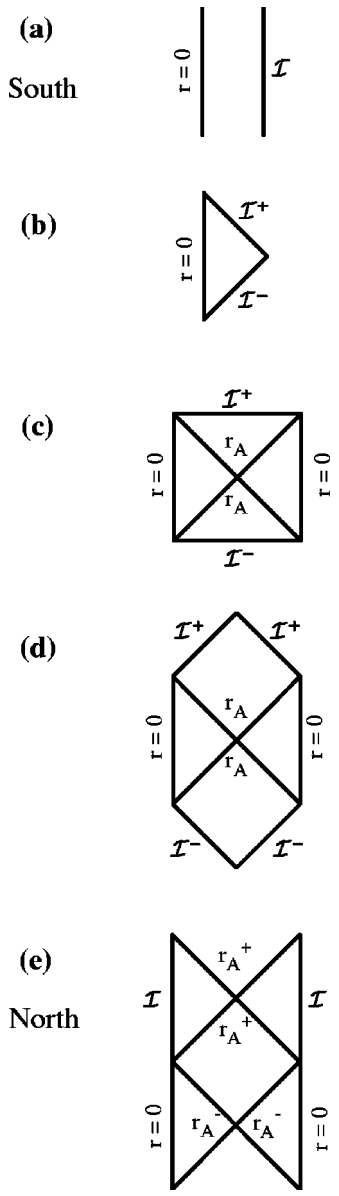

FIG. 2. Carter-Penrose diagrams of cases (a)–(e) discussed in the text of Sec. III A 1 concerning the $A > 1/\ell$, $m=0$, and $q=0$ C metric. Case (a) describes the solution seen from the vicinity of the south pole, case (c) applies to the equatorial vicinity, and case (e) describes the solution seen from the vicinity of the north pole. An accelerated horizon is represented by r_A, and $\mathcal{I}^-$ and $\mathcal{I}^+$ represent, respectively, the past and future infinity ($r=+\infty$). $r=0$ corresponds to $y=+\infty$ and $r=+\infty$ corresponds to $y=-x$.

The Kruskal coordinates in both regions were chosen in order to obtain a negative value for the factor $\mathcal{F}/(u'v')$, which appears in the metric coefficient $g_{u'v'}$. The value of constant α was selected in order that the limit of $\mathcal{F}/(u'v')$ as $y \to y_+$ stays finite and different from zero. By doing this, we have removed the coordinate singularity that was present at the root y_+ of $\mathcal{F}$ [see Eq. (17)]. So, the metric is now well-behaved in the whole range $-x \leqslant y < +\infty$ or $0 \leqslant r < +\infty$. The coordinates y and r are expressed as functions of u' and v' by Eq. (19), and at the edges of the interval allowed to r, the product $u'v'$ takes the values

$$\lim_{r\to 0} u'v' = -1,$$

$$\lim_{r\to +\infty} u'v' = \frac{y_+ + x}{y_+ - x} > 0 \text{ and finite.} \tag{26}$$

Once again, the maximal analytical extension is achieved by allowing the Kruskal coordinates u' and v' to take all the values on the range $]-\infty;+\infty[$, as soon as the condition $-1 \leqslant u'v' < (y_+ + x)/(y_+ - x)$ is satisfied. The Carter-Penrose diagram for this range of the angular direction is drawn in Fig. 2(c). $r=0$ is represented by a timelike line while $r=+\infty$ ($\mathcal{I}$) is a spacelike line. The two mutual perpendicular straight null lines at 45°, $u'v'=0$, represent the accelerated horizon at $y_A=+y_+$ or $r_A=[A(x+y_+)]^{-1}$.

(d) $x=+y_+$. In this particular direction, the region accessible to y is $-y_+ \leqslant y < +\infty$. $\mathcal{F}(y)$ is negative in region I, $-y_+ < y < y_+$, and positive in region II, $y > y_+$. It is zero at $y=+y_+$, where the only horizon (r_A) of the solution is located and $\mathcal{F}(y)$ vanishes again at $y=-y_+$, which corresponds to $r=+\infty$ (see Fig. 1). The Kruskal construction follows directly the procedure described in case (c). The only difference is that now $\lim_{r\to+\infty} u'v' = +\infty$ and thus the $r=+\infty$ line ($\mathcal{I}$) is now represented by a null line in the Carter-Penrose diagram, which is shown in Fig. 2(d).

(e) $y_+ < x \leqslant x_n$. The region accessible to y must be separated into three regions (see Fig. 1). In region I, $-x < y < -y_+$, $\mathcal{F}(y)$ is positive; in region II, $-y_+ < y < +y_+$, $\mathcal{F}(y)$ is negative; and finally in region III, $y > +y_+$, $\mathcal{F}(y)$ is positive again. We have two Rindler-like acceleration horizons, more specifically, an outer horizon at $y=-y_+$ or $r_A^+=[A(x-y_+)]^{-1}$ and an inner horizon at $y=+y_+$ or $r_A^-=[A(x+y_+)]^{-1}$. Therefore, one must introduce a Kruskal coordinate patch around each of the horizons. The first patch constructed around $-y_+$ is valid for $-x \leqslant y < +y_+$ (thus, it includes regions I and II). In region I, we define $u'=-e^{+\alpha_- u}$ and $v'=+e^{-\alpha_- v}$ so that $u'v'=-e^{-2\alpha_- y_*}$. In region II, one defines $u'=+e^{\alpha_- u}$ and $v'=+e^{-\alpha_- v}$ in order that $u'v'=+e^{-2\alpha_- y_*}$. We set $\alpha_- \equiv y_+$. Thus, in both regions I and II, the product $u'v'$ is given by

$$u'v' = -\frac{y+y_+}{y-y_+}, \tag{27}$$

and Eq. (17) expressed in terms of the Kruskal coordinates is given by

$$ds^2 = r^2\left[-\frac{(y-y_+)^2}{y_+^2}du'dv' + d\theta^2 + \sin^2\theta\, d\phi^2\right], \tag{28}$$

which is regular in this patch $-x \leqslant y < +y_+$ and, in particular, it is regular at the root $y=-y_+$ of $\mathcal{F}(y)$. However, it is singular at the second root, $y=+y_+$, of $\mathcal{F}(y)$. To regularize the metric around $y=+y_+$, one has to introduce new Kruskal coordinates for the second patch which is built around y_+ and is valid for $-y_+ < y < +\infty$ (thus, it includes regions II and III). In region II, we set $u'=+e^{-\alpha_+ u}$ and $v'=+e^{+\alpha_+ v}$ so that $u'v'=+e^{+2\alpha_+ y_*}$. In region III, one defines $u'=-e^{-\alpha_+ u}$ and $v'=+e^{+\alpha_+ v}$ in order that $u'v'=-e^{+2\alpha_+ y_*}$. We set $\alpha_+ \equiv y_+$. Thus, in both regions II and III, the product $u'v'$ is given by

$$u'v' = -\frac{y-y_+}{y+y_+}, \tag{29}$$

and, in this second Kruskal patch, Eq. (17) is given by

$$ds^2 = r^2\left[-\frac{(y+y_+)^2}{y_+^2}du'dv' + d\theta^2 + \sin^2\theta\, d\phi^2\right], \tag{30}$$

which is regular in $y > -y_+$ and, in particular, at the second root $y=+y_+$ of $\mathcal{F}(y)$. Once again, in both patches, the Kruskal coordinates were chosen in order to obtain a factor $\mathcal{F}/(u'v')$ negative [see Eq. (24)]. The values of constants α_- and α_+ were selected in order that the limit of $\mathcal{F}/(u'v')$ as $y \to \mp y_+$ stays finite and different from zero. To end the construction of the Kruskal diagram of this solution with two horizons, the two patches have to be joined together in an appropriate way first defined by Carter in the Reissner-Nordström solution.

From Eq. (29) and Eq. (27), we find the values of product $u'v'$ at the edges $r=0$ and $r=+\infty$ of the radial coordinate,

$$\lim_{r\to 0} u'v' = -1,$$

$$\lim_{r\to +\infty} u'v' = \frac{y_+ - x}{y_+ + x} < 0 \text{ and finite,} \tag{31}$$

and we conclude that both $r=0$ and $r=+\infty$ ($\mathcal{I}$) are represented by timelike lines in the Carter-Penrose diagram sketched in Fig. 2(e). The two accelerated horizons of the solution are both represented as perpendicular straight null lines at 45° ($u'v'=0$).

2. Massive uncharged solution (m>0, q=0)

Now that the causal structure of the AdS C metric with $m=0$ and $q=0$ has been studied, the construction of the Carter-Penrose diagrams for the $m>0$ case follows up directly. As was justified in detail in Sec. II C, we will consider only the case with small mass or acceleration, i.e., we require $mA < 3^{-3/2}$, in order to have compact angular surfaces (see the discussion in the text of Fig. 3). We also require that x belong to the range $[x_s, x_n]$ (see Fig. 3), where $\mathcal{G}(x) \geqslant 0$ and such that $x_s \to -1$ and $x_n \to +1$ when $mA \to 0$. By satisfying the above two conditions, we endow the $t=$const and $r=$const surfaces with the topology of a compact surface.

The technical procedure to obtain the Carter-Penrose diagrams is similar to the one described along Sec. III A 1. In what concerns the physical conclusions, we will see that the essential difference is the presence of an extra horizon, a Schwarzschild-like horizon (r_+), due to the nonvanishing mass parameter, in addition to the accelerated Rindler-like horizon (r_A), which is due to nonvanishing A. Another important difference, as stated in Sec. II B, is the presence of a

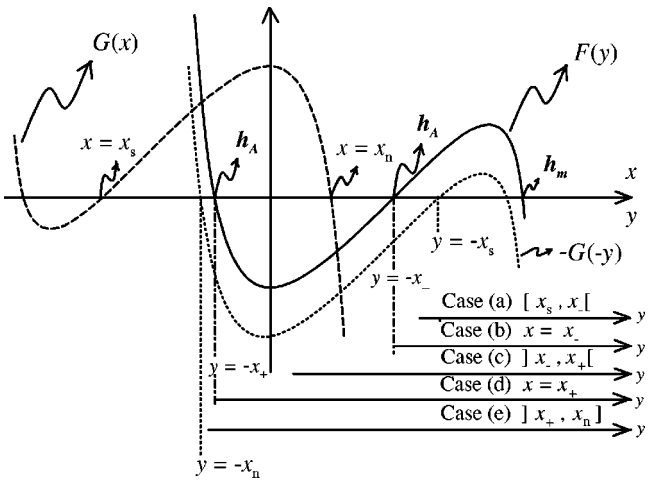

FIG. 3. Shape of $\mathcal{G}(x)$ and $\mathcal{F}(y)$ for the $A>1/\ell, mA<3^{-3/2}$, and $q=0$ C metric studied in Secs. III A 2 and IV A. The allowed range of x is between x_s and x_n, where $\mathcal{G}(x)$ is positive and compact. The permitted range of y depends on the angular direction $x(-x\leqslant y<+\infty)$ and is sketched for the five cases (a)–(e) discussed in the text. The presence of an accelerated horizon is indicated by h_A and the Schwarzschild-like horizon by h_m. [For completeness, we comment on two other cases not represented in the figure: for $A=1/\ell$, $mA<3^{-3/2}$, and $q=0$ (this case is studied in Secs. III B 2 and IV B), $\mathcal{F}(y)$ is zero at its local minimum. For $A<1/\ell$, $mA<3^{-3/2}$, and $q=0$ (this case is studied in Secs. III C 2 and IV C), the local minimum of $\mathcal{F}(y)$ is positive and only case (a) survives. For $mA=3^{-3/2}$, $\mathcal{G}(x)$ is zero at its local minimum on the left and for $mA>3^{-3/2}\mathcal{G}(x)$ is positive between $-\infty$ and x_n. These two last cases are not studied in the text.]

curvature singularity at $r=0$ and the existence of a conical singularity at the north pole (see Sec. II C).

Once more the Carter-Penrose diagrams depend on the angular direction we are looking at (see Fig. 3). We have to analyze separately five distinct cases, namely (a) $x_s\leqslant x<x_-$, (b) $x=x_-$, (c) $x_-<x<x_+$, (d) $x=x_+$, and (e) $x_+<x\leqslant x_n$, which are the massive counterparts of cases (a)–(e) that were considered in Sec. III A 1. When $m\to 0$, we have $x_s\to -1$, $x_n\to +1$, $x_-\to -y_+$, and $x_+\to +y_+$.

(a) $x_s\leqslant x<x_-$. The Carter-Penrose diagram [Fig. 4(a)] for this range of the angular direction has a spacelike curvature singularity at $r=0$, a timelike line that represents $r=+\infty$ ($\mathcal{I}$), and a Schwarzschild-like horizon (r_+) that was not present in the $m=0$ corresponding diagram Fig. 2(a). The diagram is similar to the one of the AdS-Schwarzschild solution, although now the curvature singularity has an acceleration A, as will be seen in Sec. IV.

(b) $x=x_-$. The curvature singularity $r=0$ is also a spacelike line in the Carter-Penrose diagram [see Fig. 4(b)] and there is a Schwarzschild-like horizon (r_+). The infinity, $r=+\infty$ ($\mathcal{I}$), is represented by a null line. The origin is being accelerated (see Sec. IV).

(c) $x_-<x<x_+$. The Carter-Penrose diagram [Fig. 4(c)] has a more complex structure that can be divided into left, middle, and right regions. The middle region contains the spacelike infinity ($\mathcal{I}$) and an accelerated Rindler-like horizon, $r_A=[A(x-x_-)]^{-1}$, that is already present in the $m=0$ corresponding diagram [see Fig. 2(c)]. The left and right regions both contain a spacelike curvature singularity and a Schwarzschild-like horizon, r_+.

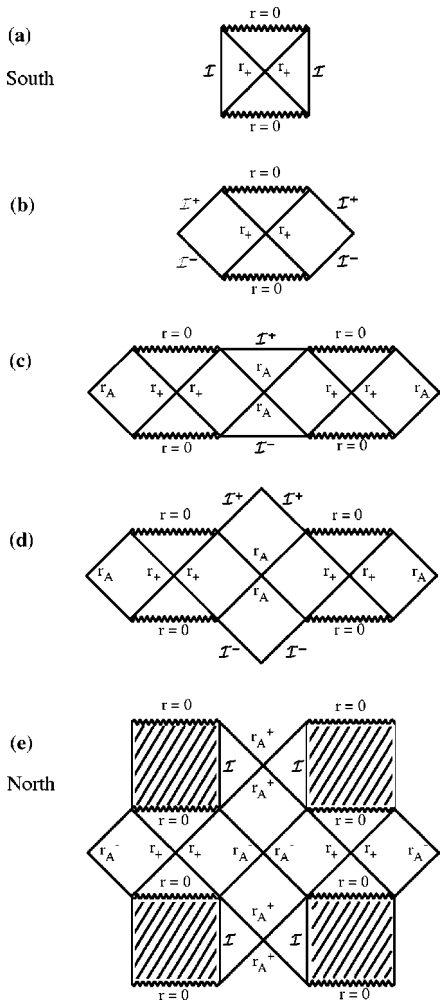

FIG. 4. Carter-Penrose diagrams of cases (a)–(e) discussed in the text of Sec. III A 2 concerning the $A>1/\ell$, $mA<3^{-3/2}$, and $q=0$ C metric. Case (a) describes the solution seen from the vicinity of the south pole, case (c) applies to the equatorial vicinity, and case (e) describes the solution seen from the vicinity of the north pole. The zigzag line represents a curvature singularity, an accelerated horizon is represented by r_A, the Schwarzschild-like horizon is sketched as r_+, $r=0$ corresponds to $y=+\infty$, and $r=+\infty$ ($\mathcal{I}$) corresponds to $y=-x$. The hatched region does not belong to the solution. In diagrams (c)–(e) we have to glue indefinitely copies of the represented figure in the left and right sides of it. In diagram (e) a similar gluing must be done in the top and bottom regions.

(d) $x=x_+$. The Carter-Penrose diagram [Fig. 4(d)] for this particular value of the angular direction is similar to that of case (c). The only difference is that $r=+\infty$ ($\mathcal{I}$) is represented by a null line rather than a spacelike line.

(e) $x_+<x\leqslant x_n$. The Carter-Penrose diagram [Fig. 4(e)] can again be divided into left, middle, and right regions. The middle region consists of a timelike line representing $r=+\infty$ ($\mathcal{I}$) and two accelerated Rindler-like horizons, an inner one ($r_A^-=[A(x-x_-)]^{-1}$) and an outer one ($r_A^+=[A(x-x_+)]^{-1}$), that were already present in the $m=0$ corre-

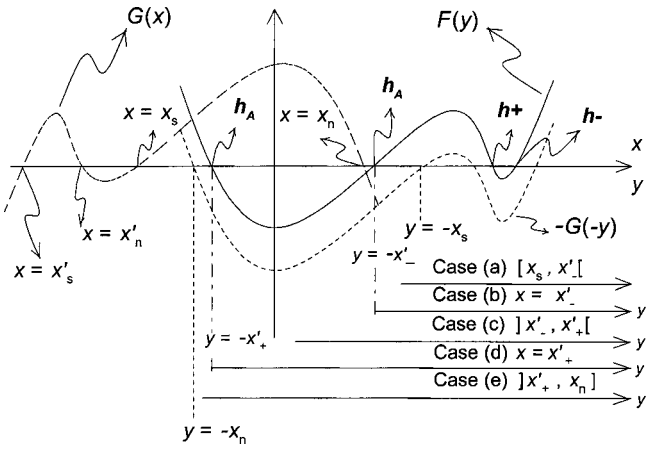

FIG. 5. Shape of $\mathcal{G}(x)$ and $\mathcal{F}(y)$ for the nonextremal charged massive *C*-metric (with $A>1/\ell$) studied in Secs. III A 3 and IV A. The allowed range of x is between x_s and x_n, where $\mathcal{G}(x)$ is positive and compact. The permitted range of y depends on the angular direction $x(-x\leqslant y<+\infty)$ and is sketched for the five cases (a)–(e) discussed in the text. The presence of an accelerated horizon is indicated by h_A and the inner and outer charged horizons by $h-$ and $h+$. In the extremal case, $h-$ and $h+$ superpose each other and in the naked case $\mathcal{F}(y)>0$ in the local minimum on the right. [For completeness, we comment on two other cases not represented in the figure: for $A=1/\ell$ (this case is studied in Secs. III B 3 and IV B), $\mathcal{F}(y)$ is zero at its local minimum on the left. For $A<1/\ell$ (this case is studied in Secs. III C 3 and IV C), the local minimum on the left of $\mathcal{F}(y)$ is positive and only case (a) survives.]

sponding diagram [Fig. 2(e)]. The left and right regions both contain a spacelike curvature singularity and a Schwarzschild-like horizon (r_+).

3. Massive charged solution (m>0, q≠0)

When both the mass and charge parameters are nonzero, depending on the values of the parameters A, m, and q, $\mathcal{G}(x)$ can be positive in a single compact interval, $]x_s,x_n[$, or in two distinct compact intervals, $]x_s',x_n'[$ and $]x_s,x_n[$, say (see Fig. 5). In this latter case, we will work only with the interval $[x_s,x_n]$ (say) for which the charged solutions are in the same sector of those we have analyzed in the last two subsections when $q\to 0$.

Depending also on the values of A, m, and q, the function $\mathcal{F}(y)$ can have four roots, three roots (one of them degenerated), or two roots (see the discussion in the text of Fig. 5). As will be seen, the first case describes a pair of accelerated AdS–Reissner-Nordström (AdS-RN) black holes, the second case describes a pair of extremal AdS-RN black holes, and the third case describes a pair of naked AdS-RN singularities.

The essential differences between the Carter-Penrose diagrams of the massive charged solutions and those of the massive uncharged solutions are (i) the curvature singularity is now represented by a timelike line rather than a spacelike line, and (ii) excluding the extremal and naked cases, there are now (in addition to the accelerated Rindler-like horizon, r_A) not one but two extra horizons, the expected inner (r_-) and outer (r_+) horizons associated to the charged character of the solution.

Below, we study the causal structure of the electric or magnetic counterparts of cases (a)–(e) discussed in the last two sections (see Fig. 5), namely (a) $x_s\leqslant x<x_-'$, (b) $x=x_-'$, (c) $x_-'<x<x_+'$, (d) $x=x_+'$ and (e) $x_+'<x\leqslant x_n$. When $q\to 0$, we have $x_-'\to x_-$ and $x_+'\to x_+$. The Carter-Penrose diagrams are drawn in Fig. 6. In these diagrams, the left column represents the nonextremal case, the middle column represents the extremal case, and the right column represents the naked charged case. Row (a) describes the solution seen from the vicinity of the south pole, row (c) applies to the equatorial vicinity, and row (e) describes the solution seen from the vicinity of the north pole. The zigzag line represents a curvature singularity, an accelerated horizon is represented by r_A, and the inner and outer charge associated horizons are sketched as r_- and r_+. $\mathcal{I}^-$ and $\mathcal{I}^+$ represent, respectively, the past and future infinity $(r=+\infty)$. $r=0$ corresponds to $y=+\infty$ and $r=+\infty$ corresponds to $y=-x$. The hatched region does not belong to the solution. In diagrams (c)–(e), we have to glue indefinitely copies of the represented figure on the left and right sides of it. In some of the diagrams, a similar gluing must be done in the top and bottom regions.

(a) $x_s\leqslant x<x_-'$. Both the curvature singularity, $r=0$, and $r=+\infty$ $(\mathcal{I})$ are represented by a spacelike line in the Carter-Penrose diagram [Fig. 6(a)]. Besides, in the nonextremal case, there is an inner horizon (r_-) and an outer horizon (r_+) associated with the charged character of the solution. In the extremal case, the two horizons r_- and r_+ become degenerate and so there is a single horizon, r_+ (say), and in the naked case there is no horizon. The diagram is similar to that of the AdS–Reissner-Nordström solution, although now the curvature singularity has an acceleration A, as will be seen in Sec. IV.

(b) $x=x_-'$. The curvature singularity $r=0$ is a spacelike line in the Carter-Penrose diagram [see Fig. 6(b)] and $r=+\infty$ $(\mathcal{I})$ is represented by a null line. Again, in the nonextremal case, there is an inner horizon (r_-) and an outer horizon (r_+) associated to the charged character of the solution. In the extremal case, there is a single horizon, r_+, and in the naked case there is no horizon. The origin is being accelerated (see Sec. IV).

(c) $x_-'<x<x_+'$. The Carter-Penrose diagram [Fig. 6(c)] has a complex structure. As before [see Fig. 4(c)], it can be divided into left, middle, and right regions. The middle region contains the spacelike infinity $(\mathcal{I})$ and an accelerated Rindler-like horizon, $r_A=[A(x-x_-')]^{-1}$, that was already present in the $m=0$, $q=0$ corresponding diagram [see Fig. 2(c)]. The left and right regions both contain a timelike curvature singularity $(r=0)$. In addition, in the nonextremal case these left and right regions contain an inner horizon (r_-) and an outer horizon (r_+), in the extremal case they contain a single horizon (r_+), and in the naked case they have no horizon.

(d) $x=x_+'$. The Carter-Penrose diagram [Fig. 6(d)] for this particular value of the angular direction is similar that of case (c). The only difference is that $r=+\infty$ $(\mathcal{I})$ is represented by a null line rather than a spacelike line.

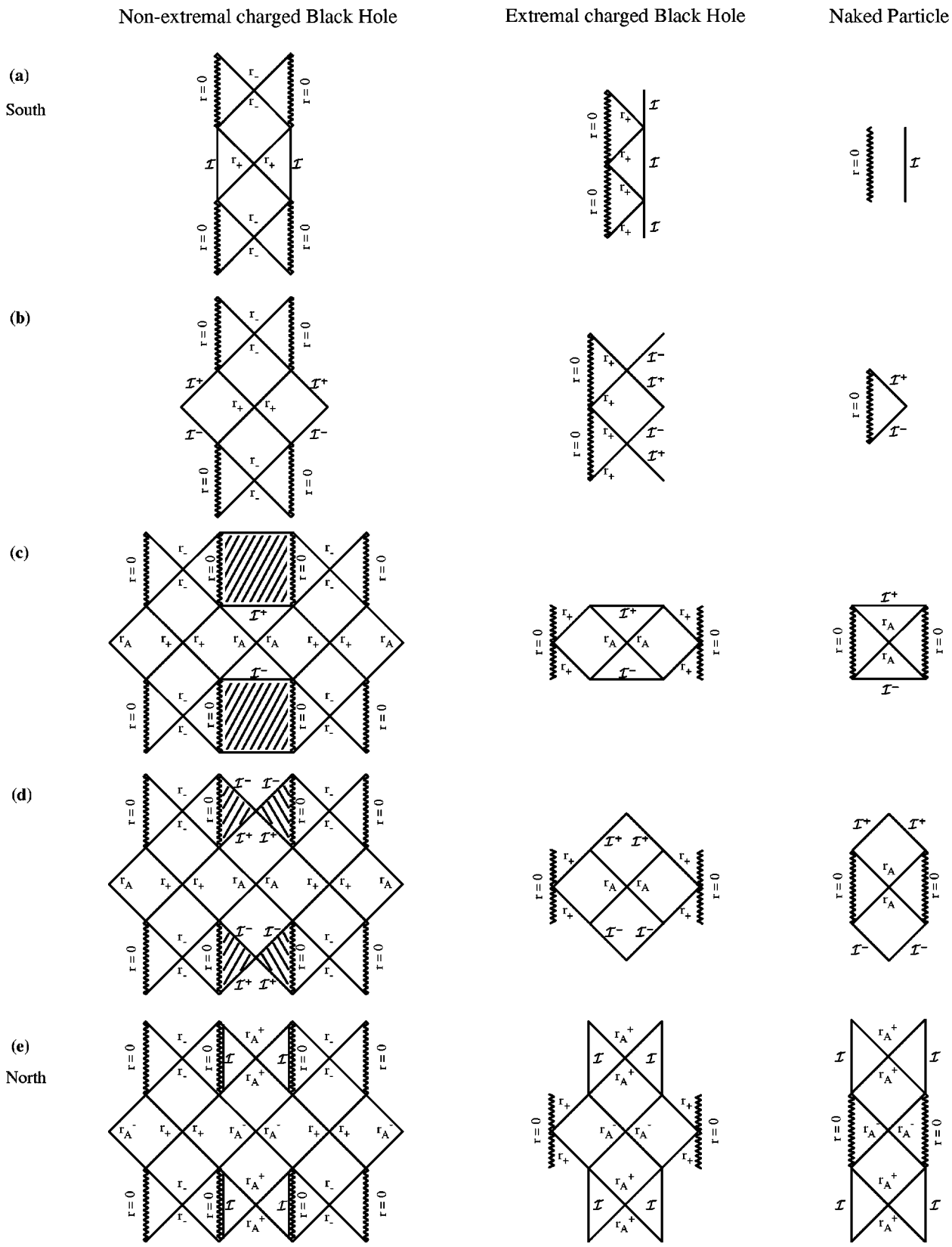

FIG. 6. Carter-Penrose diagrams of cases (a)–(e) discussed in the text of Sec. III A 3 concerning the charged massive *C* metric. The left column represents the nonextremal case, the middle column represents the extremal case, and the right column represents the naked charged case. Row (a) describes the solution seen from the vicinity of the south pole, row (c) applies to the equatorial vicinity, and row (e) describes the solution seen from the vicinity of the north pole.

(e) $x'_+ < x \leqslant x_n$. The Carter-Penrose diagram [Fig. 6(e)]. As before [see Fig. 4(e)], it can be divided into left, middle, and right regions. The middle region consists of a timelike line representing $r=+\infty$ ($\mathcal{I}$) and two accelerated Rindler-like horizons, $r_A^- = [A(x-x'_-)]^{-1}$ and $r_A^+ = [A(x-x'_+)]^{-1}$, that were already present in the $m=0$ and $q=0$ corresponding diagram [see Fig. 2(e)]. The left and right regions both contain a timelike curvature singularity ($r=0$). In addition, in the nonextremal case these left and right regions contain an inner horizon (r_-) and an outer horizon (r_+), in the extremal case they contain a single horizon (r_+), and in the naked case they have no horizon (see, however, the physical interpretation of this case as a black hole at the end of Sec. IV A 3).

B. Causal structure of the $A=1/\ell$ solutions

The $A=1/\ell$ case was studied in detail in [22]. In particular, the causal structure of the massive uncharged solution was discussed. For completeness, we will also present the causal diagrams of the massless uncharged solution and of the massive charged solution.

Once more, due to the lower restriction on the value of y ($-x \leqslant y$), the causal diagrams depend on the angular direction x we are looking at. We have to consider separately three distinct sets of angular directions (see the discussion in the text of Figs. 1, 3, and 5), namely (a) $x_s \leqslant x < 0$, (b) $x=0$, and (c) $0 < x \leqslant x_n$, where $x_s=-1$ and $x_n=+1$ when $m=0$ and $q=0$.

1. Massless uncharged solution (m=0, q=0)

In this case, we have $x \in [x_s=-1, x_n=+1]$, $x=\cos\theta$, $\mathcal{G} = 1-x^2 = \sin^2\theta$, $\kappa=1$, and $\mathcal{F}(y)=y^2$ (see the discussion in the text of Fig. 1). The angular surfaces Σ ($t=$const and $r=$const) are spheres free of conical singularities. The origin of the radial coordinate r has no curvature singularity and therefore both r and y can lie in the range $]-\infty,+\infty[$. However, in the general case, where m or q are nonzero, there is a curvature singularity at $r=0$. Since the discussion of the present section is only a preliminary to that of the massive general case, following [6], we will treat the origin $r=0$ as if it had a curvature singularity and thus we admit that r belongs to the range $[0,+\infty[$ and y lies in the region $-x \leqslant y < +\infty$. The Carter-Penrose diagrams are drawn in Fig. 7. In case (c), $0 < x \leqslant x_n$, and only in this case is there an accelerated horizon, $r_A = (Ax)^{-1}$.

2. Massive uncharged solution (m>0, q=0)

The causal diagrams of this solution were first presented in [22] and are drawn in Fig. 8. In the case (c), $0 < x \leqslant x_n$, and only in this case is there an accelerated horizon, $r_A = (Ax)^{-1}$ which is degenerated (see [22]). The Schwarzschild-like horizon is at $r_+ = A^{-1}[x + 1/(2mA)]^{-1}$.

3. Massive charged solution (m>0, q≠0)

The Carter-Penrose diagrams of the solution for this range of parameters are sketched in Fig. 9. In these diagrams, the left column represents the nonextremal black hole, the middle column represents the extremal black hole, and the right column represents the naked charged particle. Row (a) describes the solution seen from an angle that is between the south pole (including) and the equator (excluding), row (b) applies only to the equatorial direction, and row (c) describes the solution seen from an angle between the equator (excluding) and the north pole (including).

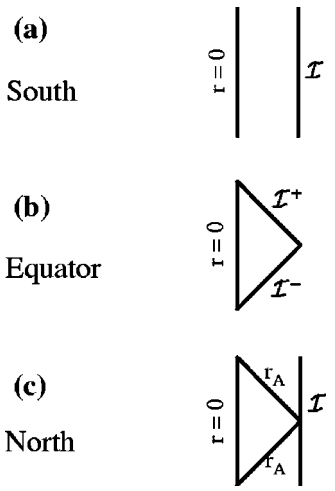

FIG. 7. Carter-Penrose diagrams of cases (a)–(c) discussed in the text of Sec. III B 1 concerning the $A=1/\ell$, $m=0$, and $q=0$ C metric. $r_A=(Ax)^{-1}$. In diagrams (a) and (c) we have to glue indefinitely copies of the represented figure in the top and bottom regions of it.

C. Causal structure of the $A<1/\ell$ solutions

The $A<1/\ell$ case was first analyzed in [23]. We complement it with the analysis of the causal structure. Contrary to the cases $A>1/\ell$ and $A=1/\ell$, the causal diagrams of this spacetime do not depend on the angular direction we are

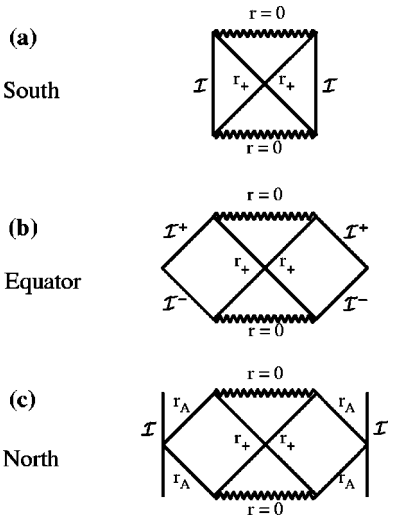

FIG. 8. Carter-Penrose diagrams of cases (a)–(c) discussed in the text of Sec. III B 2 concerning the $A=1/\ell$, $mA<3^{-3/2}$, and $q=0$ C metric. $r_A=(Ax)^{-1}$ is a degenerated horizon (see [22]). In diagram (c) we have to glue indefinitely copies of the represented figure in the top and bottom regions of it.

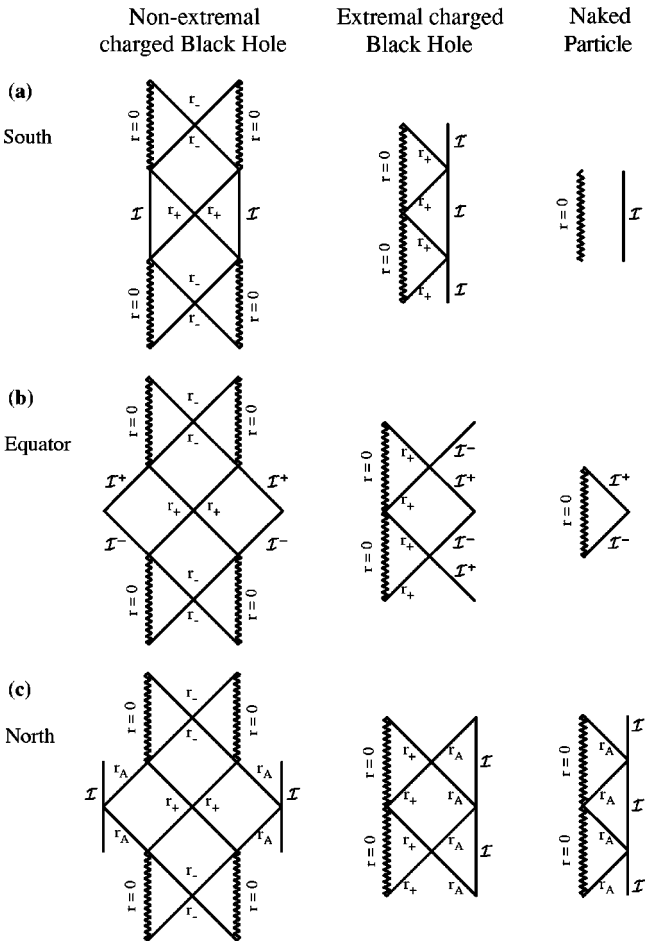

FIG. 9. Carter-Penrose diagrams of cases (a)–(c) discussed in the text of Sec. III B 3 concerning the charged massive *C* metric with $A=1/\ell$. The left column represents the nonextremal black hole, the middle column represents the extremal black hole, and the right column represents the naked charged particle. $r_A=(Ax)^{-1}$ is an accelerated horizon and r_- and r_+ are charged associated horizons. In these diagrams we have to glue indefinitely copies of the represented figure in the top and bottom regions of it.

looking at. The reason for this feature is clearly identified and explained in the discussion in the text of Figs. 1, 3, and 5.

1. Massless uncharged solution (m=0, q=0)

The Carter-Penrose diagram is identical to that of the AdS solution ($A=0$, $m=0$, $q=0$) and is sketched in Fig. 7(a). The origin has an acceleration *A*, as will be seen in Sec. IV.

2. Massive uncharged solution (m>0, q=0)

The Carter-Penrose diagram is identical to that of the AdS-Schwarzschild solution ($A=0$, $m>0$, $q=0$) and is drawn in Fig. 8(a). The origin has an acceleration *A*, as will be seen in Sec. IV.

3. Massive charged solution (m>0, q≠0)

The Carter-Penrose diagrams are identical to those of the AdS–Reissner-Nordström solution ($A=0$, $m>0$, $q\neq 0$) and are represented in Fig. 9(a). In this figure, the nonextremal black hole is represented in the left column, the extremal black hole is represented in the middle column, and the naked charged particle is represented in the right column. The origin has an acceleration *A*, as will be seen in Sec. IV.

IV. PHYSICAL INTERPRETATION OF THE AdS *C* METRIC

The parameter *A* that is found in the AdS *C* metric is interpreted as being an acceleration and the AdS *C* metric with $A>1/\ell$ describes a pair of black holes accelerating away from each other in an AdS background, while the AdS *C* metric with $A\leqslant 1/\ell$ describes a single accelerated black hole. In this section, we will justify this statement.

In the Appendix it is shown that, when $A=0$, the general AdS *C* metric, Eq. (13), reduces to the AdS ($m=0$, $q=0$), to the AdS-Schwarzschild ($m>0$, $q=0$), and to the AdS–Reissner-Nordström solutions ($m=0$, $q\neq 0$). Therefore, the parameters *m* and *q* are, respectively, the ADM mass and ADM electromagnetic charge of the nonaccelerated black holes. Moreover, if we set the mass and charge parameters equal to zero, even when $A\neq 0$, the Kretschmann scalar [see Eq. (7)] reduces to the value expected for the AdS spacetime. This indicates that the massless uncharged AdS *C* metric is an AdS spacetime in disguise.

A. $A>1/\ell$: Pair of accelerated black holes

In this section, we will first interpret case 1. [Massless uncharged solution ($m=0$, $q=0$)], which is the simplest, and then with the acquired knowledge we interpret cases 2 [massive uncharged solution ($m>0$, $q=0$)] and 3. [massive charged solution ($m>0$, $q\neq 0$)]. We will interpret the solution following two complementary descriptions, the four dimensional (4D) one and the five dimensional (5D) one.

1. The four-dimensional description (m=0, q=0)

As we said in Sec. III A 1, when $m=0$ and $q=0$, the origin of the radial coordinate *r* defined in Eq. (6) has no curvature singularity and therefore *r* has the range $]-\infty, +\infty[$. However, in the realistic general case, where *m* or *q* are nonzero, there is a curvature singularity at $r=0$ and since the discussion of the massless uncharged solution was only a preliminary to that of the massive general case, following [6], we have treated the origin $r=0$ as if it had a curvature singularity and thus we admitted that *r* belongs to the range $[0,+\infty[$. In these conditions, we obtained the causal diagrams of Fig. 2. Note, however, that one can make a further extension to include the negative values of *r*, enlarging in this way the range accessible to the Kruskal coordinates u' and v'. By doing this procedure, we obtain the causal diagram of the AdS spacetime. In Fig. 10, we show the extension to negative values of coordinate *r* (so $-\infty<y<+\infty$) of the Carter-Penrose diagrams of Fig. 2. This diagram indicates that the origin of the AdS spacetime, $r=0$, is accelerating. The situation is analogous to the one that occurs in the usual Rindler spacetime, $ds^2=-X^2dT^2+dX^2$. If one restricts the coordinate *X* to be positive, one obtains an accelerated origin that approaches a Rindler accelerated horizon.

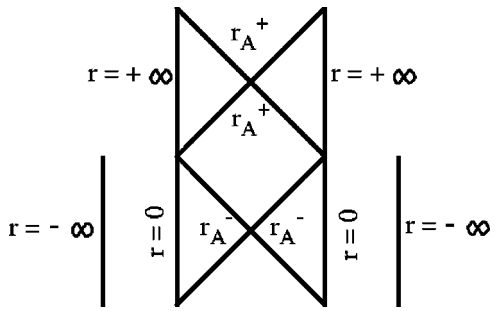

FIG. 10. Extending the Carter-Penrose diagrams of Fig. 2 to negative values of r, we obtain the AdS spacetime with its origin being accelerated. $r_A^+=[A(x-y_+)]^{-1}>0$ and $r_A^-=[A(x+y_+)]^{-1}>0$. We have to glue indefinitely copies of the represented figure in the top and bottom regions.

However, by making an extension to negative values of X one obtains the Minkowski spacetime.

Now, we want to clearly identify the parameter A that appears in the AdS C metric with the acceleration of its origin. To achieve this aim, we recover the massless uncharged AdS C metric defined by Eq. (3) and Eq. (4) (with $m=0$ and $q=0$), and after performing the following coordinate transformation:

$$\tau=\frac{\sqrt{\ell^2A^2-1}}{A}t,\quad \rho=\frac{\sqrt{\ell^2A^2-1}}{A}\frac{1}{y},$$

$$\theta=\arccos x,\qquad \phi=z, \tag{32}$$

we can rewrite the massless uncharged AdS C metric as

$$ds^2=\frac{1}{\gamma^2}\left[-(1-\rho^2/\ell^2)d\tau^2+\frac{d\rho^2}{1-\rho^2/\ell^2}+\rho^2d\Omega^2\right], \tag{33}$$

with $d\Omega^2=d\theta^2+\sin^2\theta d\phi^2$ and

$$\gamma=\sqrt{\ell^2A^2-1}+A\rho\cos\theta. \tag{34}$$

The causal diagram of this spacetime is drawn in Fig. 11. Notice that the origin of the radial coordinate ρ corresponds to $y=+\infty$ and therefore to $r=0$, where r has been introduced in Eq. (6). So, when we consider the massive AdS C metric there will be a curvature singularity at $\rho=0$ (see Sec. II B).

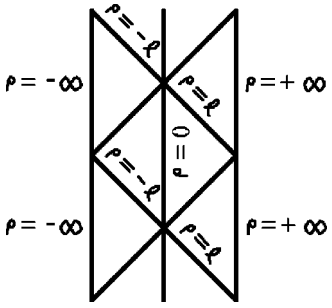

FIG. 11. Carter-Penrose diagram of metric (33). We have to glue indefinitely copies of the represented figure in the top and bottom regions.

To discover the meaning of parameter A we consider the 4D timelike worldlines described by an observer with $\rho=$const, $\theta=0$, and $\phi=0$ (see [28]). These are given by $x^\mu(\lambda)=(\gamma\ell\lambda/\sqrt{\ell^2-\rho^2},\rho,0,0)$, where λ is the proper time of the observer since the 4-velocity $u^\mu=dx^\mu/d\lambda$ satisfies $u_\mu u^\mu=-1$. The 4-acceleration of these observers, $a^\mu=(\nabla_\nu u^\mu)u^\nu$, has a magnitude given by

$$|a_4|=\sqrt{a_\mu a^\mu}=\frac{\rho\sqrt{\ell^2A^2-1}+\ell^2A}{\ell\sqrt{\ell^2-\rho^2}}. \tag{35}$$

Since $a_\mu u^\mu=0$, the value $|a_4|$ is also the magnitude of the 3-acceleration in the rest frame of the observer. From Eq. (35) we achieve the important conclusion that the origin of the AdS C metric, $\rho=0$ (or $r=0$), is being accelerated with a constant acceleration whose value is precisely given by the parameter A that appears in the AdS C metric. Moreover, at radius $\rho=\ell$ [or $y=y_+$ defined in Eq. (14)] the acceleration is infinite, which corresponds to the trajectory of a null ray. Thus, observers held at $\rho=$const see this null ray as an acceleration horizon and they will never see events beyond this null ray.

2. The five-dimensional description (m=0, q=0)

In order to improve and clarify the physical aspects of the AdS C metric, we turn now to the 5D representation of the solution.

The AdS spacetime can be represented as the 4-hyperboloid,

$$-(z^0)^2+(z^1)^2+(z^2)^2+(z^3)^2-(z^4)^2=-\ell^2, \tag{36}$$

in the 5D Minkowski (with two timelike coordinates) embedding spacetime,

$$ds^2=-(dz^0)^2+(dz^1)^2+(dz^2)^2+(dz^3)^2-(dz^4)^2. \tag{37}$$

Now, the massless uncharged AdS C metric is an AdS spacetime in disguise and therefore our next task is to understand how the AdS C metric can be described in this 5D picture. To do this, we first recover the massless uncharged AdS C metric described by Eq. (33) and apply to it the coordinate transformation,

$$\begin{aligned}
z^0&=\gamma^{-1}\sqrt{\ell^2-\rho^2}\sinh(\tau/\ell),\\
z^1&=\gamma^{-1}\sqrt{\ell^2-\rho^2}\cosh(\tau/\ell),\\
z^2&=\gamma^{-1}\rho\sin\theta\cos\phi,\\
z^3&=\gamma^{-1}\rho\sin\theta\sin\phi,\\
z^4&=\gamma^{-1}[\sqrt{\ell^2A^2-1}\rho\cos\theta+\ell^2A],
\end{aligned} \tag{38}$$

where γ is defined in Eq. (34). Transformations (38) define an embedding of the massless uncharged AdS C metric into

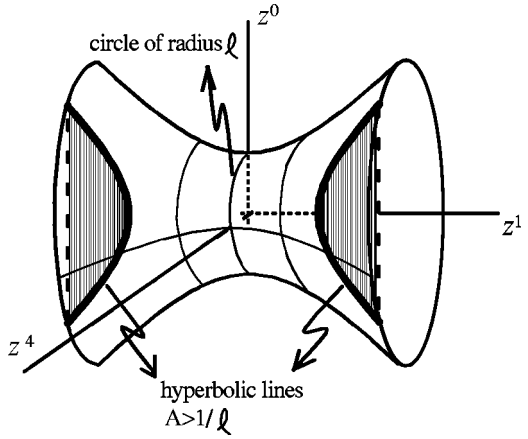

FIG. 12. AdS 4-hyperboloid embedded in the 5D Minkowski spacetime with two timelike coordinates, z^0 and z^4. The directions z^2 and z^3 are suppressed. The two hyperbolic lines lying on the AdS hyperboloid result from the intersection of the hyperboloid surface with the $z^4=\text{const}>\ell$ plane. They describe the motion of the origin of the AdS C metric with $A>1/\ell$.

the 5D description of the AdS spacetime since they satisfy Eq. (36) and take directly Eq. (33) into Eq. (37).

So, the massless uncharged AdS C metric is an AdS spacetime, but we can extract more information from this 5D analysis. Indeed, let us analyze with some detail the properties of the origin of the radial coordinate, $\rho=0$ (or $r=0$). This origin moves in the 5D Minkowski embedding spacetime according to [see Eq. (38)]

$$z^2=0,\ \ z^3=0,\ \ z^4=\ell^2 A/\sqrt{\ell^2A^2-1}>\ell,$$

and

$$(z^1)^2-(z^0)^2=(A^2-1/\ell^2)^{-1}\equiv a_5^{-2}. \tag{39}$$

These equations define two hyperbolic lines lying on the AdS hyperboloid which result from the intersection of this hyperboloid surface defined by Eq. (36) and the $z^4=\text{const}>\ell$ plane (see Fig. 12). They tell us that the origin is subjected to a uniform 5D acceleration, a_5, and consequently moves along a hyperbolic worldline in the 5D embedding space, describing a Rindler-like motion (see Figs. 12 and 13) that resembles the well-known hyperbolic trajectory, $X^2-T^2=a^{-2}$, of an accelerated observer in Minkowski space. But uniformly accelerated radial worldlines in the 5D Minkowski embedding space are also uniformly accelerated worldlines in the 4D AdS space [29], with the 5D acceleration a_5 being related to the associated 4D acceleration a_4 by $a_5^2=a_4^2-1/\ell^2$. Comparing this last relation with Eq. (39) we conclude that $a_4\equiv A$. Therefore, and once again, we conclude that the origin of the AdS C metric is uniformly accelerating with a 4D acceleration whose value is precisely given by the parameter A that appears in the AdS C metric, Eq. (3), and this solution describes an AdS space whose origin is not at rest as usual but is being accelerated. Note that the origin of the usual AdS spacetime describes the circle $(z^0)^2+(z^4)^2=\ell^2$ in the AdS hyperboloid in contrast to the origin of the AdS C metric with $A>1/\ell$, whose motion is described by

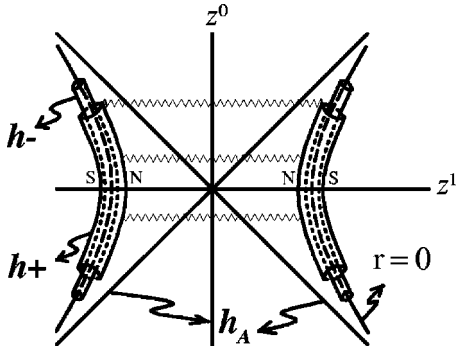

FIG. 13. Schematic diagram representing the 5D hyperbolic motion of two uniformly accelerating massive charged black holes approaching asymptotically the Rindler-like accelerated horizon (h_A). The inner and outer charged horizons are represented by $h-$ and $h+$. The strut that connects the two black holes is represented by the zigzag lines. The north pole direction is represented by N and the south pole direction by S.

Eq. (39). This discussion allowed us to find the physical interpretation of parameter A and to justify its label. Notice also that the original AdS C metric coordinates introduced in Eq. (3) cover only the half-space $z^1>-z^0$. The Kruskal construction done in Sec. III A extended this solution to include also the $z^1<-z^0$ region and so, in the extended solution, $r=0$ is associated to two hyperbolas that represent two accelerated points (see Fig. 13). These two hyperbolas approach asymptotically the Rindler-like acceleration horizon (r_A), so called because it is is absent when $A=0$ and present even when $A\neq 0$, $m=0$, and $q=0$.

3. Pair of accelerated black holes ($m>0$, $q\neq 0$)

Now, we are in position to interpret the massive and charged solutions that describe two black holes accelerating away from each other. To see this clearly, let us look to the Carter-Penrose diagrams near the equator, Fig. 2(c), Fig. 4(c), and Fig. 6(c) [for the discussion that follows, we could, as well, look at the diagrams of case (d) in these figures]. Looking at these figures, we can compare the different features that belong to the massless uncharged case [Fig. 2(c)], to the massive uncharged case [Fig. 4(c)], and ending in the massive charged case [Fig. 6(c)]. In Fig. 2(c), we identify the two hyperbolas $r=0$ (represented by two timelike lines) approaching asymptotically the Rindler-like acceleration horizon (r_A). When we add a mass to the solution we conclude that each of these two simple hyperbolas $r=0$ are replaced by the more complex structure that represents a Schwarzschild black hole with its spacelike curvature singularity and its horizon [these are represented by r_+ in the left and right regions of Fig. 4(c)]. So, the two accelerating points $r=0$ have been replaced by two Schwarzschild black holes that approach asymptotically the Rindler-like acceleration horizon [represented by r_A in the middle region of Fig. 4(c)]. The same interpretation can be assigned to the massive charged solution. The two hyperbolas $r=0$ of Fig. 2(c) are replaced by two Reissner-Nordström black holes [with its timelike curvature singularity and its inner r_- and outer r_+ horizons; see the left and right regions of Fig. 6(c)] that approach

asymptotically the Rindler-like acceleration horizon already present in the $m=0$ and $q=0$ causal diagram.

The Carter-Penrose diagrams of cases (a) and (b) of Fig. 4 and Fig. 6 indicate that an observer that is looking through an angular direction which is in the vicinity of the south pole does not see the acceleration horizon and notices the presence of a single black hole. This is in agreement with Fig. 13. Indeed, in this schematic figure, coordinates z^0 and z^1 can be seen as Kruskal coordinates and we conclude that an observer, initially located at infinity ($z^1=\infty$) and moving inwards into the black hole along the south pole, passes through the black hole horizons and hits eventually its curvature singularity. Therefore, he never has the opportunity of getting in contact with the acceleration horizon and with the second black hole. This is no longer true for an observer that moves into the black hole along an angular direction that is in the vicinity of the north pole. In Fig. 13 this observer would be between the two black holes, at one of the points of the $z^0<0$ semiaxis (say) and moving into the black hole. Clearly, this observer passes through the acceleration horizon before crossing the black hole horizons and hitting its curvature singularity. This description agrees with cases (c), (d), and (e) of Fig. 4 and Fig. 6, which describe the solution along an angular direction which includes the equatorial plane [case (c)] as well as the north pole [case (e)].

The diagrams of the third column of Fig. 6 concerning the naked case of the $A>1/\ell$ massive charged C metric deserve a comment. First, we stress that the term ''naked'' is employed in this situation because the values of parameters m and q are such that the solution has no charged associated horizons, i.e., in the notation used in this paper, r_- and r_+ are not present in these diagrams. However, these diagrams present an interesting new feature. Indeed, looking at rows (a) and (b) we have a single accelerated naked particle, in rows (c) and (d) we find two naked singularities approaching asymptotically the acceleration horizon r_A, but in row (e) we no longer have two naked singularities. More precisely, we have a kind of single AdS-Reissner-Nordström black hole with the curvature singularity being provided by the mass and charge but with the horizons having their origin in the acceleration and cosmological constant.

4. Source of acceleration: The strut

We can now ask, what entity is causing the acceleration and where is it localized? To achieve this aim, let us go back to the massless uncharged AdS C metric and consider radial worldlines motions with $z^2=0$, $z^3=0$, and $z^4=$const or, equivalently, with $\theta=0$, $\phi=$const, and $\rho=$const. These observers move along a Rindler-like hyperbola described by [see Eq. (38)]

$$(z^1)^2-(z^0)^2=\frac{\ell^2-\rho^2}{(\sqrt{\ell^2A^2-1}+A\rho)^2}. \tag{40}$$

Since the right-hand side of Eq. (40) is smaller than a_5^{-2} defined in Eq. (39), the north pole $\theta_n=0$ is localized between the hyperbolas $(z^1)^2-(z^0)^2=a_5^{-2}$ in the z^0,z^1 diagram (see Fig. 13). What does this means? When we put m or q different from zero, each of the two hyperbolas assigned to $r=0$ represent the accelerated motion of a black hole. Thus, Eq. (40) tells us that the $\theta_n=0$ axis points toward the other black hole, i.e., it is in the region between the two black holes (see Fig. 13). The south pole points along the symmetry axis towards spatial infinity. Now, in Sec. II C, we saw that parameter κ has been chosen in order to avoid a conical singularity at the south pole [see Eq. (12)] and, by doing so, at the north pole a conical singularity is localized. This is associated with a strut that joins the two black holes and provides the acceleration of the black holes. To confirm this, recall that either a straight string or a strut has a metric described by [30,31]

$$ds^2=-dt^2+dZ^2+d\varrho^2+\varrho^2d\tilde{\phi}^2, \tag{41}$$

where $\tilde{\phi}=[1-\delta/(2\pi)]\phi$ and $0\leqslant\phi<2\pi$. A string has $\delta>0$ and the geometry around it is conic, i.e., it is a plane with a deficit angle δ, while a strut has $\delta<0$. Their mass per unit length is $\mu=\delta/(8\pi)$ and their interior energy-momentum tensor is

$$T_\alpha{}^\beta=\mu\,\delta(X)\,\delta(Y)\,\mathrm{diag}(-1,0,0,-1), \tag{42}$$

where $X=\varrho\cos\tilde{\phi}$ and $Y=\varrho\sin\tilde{\phi}$ are the directions normal to the strut, and $\delta(X)$ and $\delta(Y)$ are Dirac delta functions. The pressure on the string or in the strut satisfies $p=-\mu$. If $\mu>0$, we have a string; if $\mu<0$, we have a strut. Now, turning to our case, the AdS C metric, Eq. (13), near the north pole is given by

$$ds^2\sim-r^2\mathcal{F}dt^2+r^2\mathcal{F}^{-1}dy^2+\left(r^2d\theta^2+\frac{\kappa^2}{4}\left|\frac{dG}{dx}\right|_{x_n}r^2\theta^2d\phi^2\right), \tag{43}$$

where κ is defined in Eq. (12) and the term between the parentheses brackets is the induced metric in the plane normal to the strut that connects the two black holes (along the y direction) and will be labeled as dX^2+dY^2. The C-metric strut has a mass per unit length given by

$$\mu=\frac{1}{4}\frac{\delta_n}{2\pi}=\frac{1}{4}\left(1-\left|\frac{d\mathcal{G}}{dx}\right|_{x_s}^{-1}\left|\frac{d\mathcal{G}}{dx}\right|_{x_n}\right). \tag{44}$$

We have $|d_x\mathcal{G}|_{x_s}<|d_x\mathcal{G}|_{x_n}$ and so μ is negative. To obtain the pressure of the C-metric strut, we write Eq. (43) in a Minkowski frame, $ds^2=-\theta^{(0)2}+\theta^{(1)2}+\theta^{(2)2}+\theta^{(3)2}$, with $\theta^{(A)}=e^{(A)}{}_\alpha dx^\alpha$ and $e^{(0)}{}_0=r\sqrt{\mathcal{F}}$, $e^{(1)}{}_1=r$, $e^{(2)}{}_2=r\,\theta k|d_x\mathcal{G}|_{x_n}/2$, and $e^{(3)}{}_3=r/\sqrt{\mathcal{F}}$. In this Minkowski frame the energy-momentum tensor, $T_{(A)}{}^{(B)}$, of the C-metric strut is given by Eq. (42). In order to come back to the coordinate basis frame and write the energy-momentum tensor of the C-metric strut in this basis, we use $T^{\alpha\beta}=e^{(A)\alpha}e_{(B)}{}^\beta T_{(A)}{}^{(B)}$ and obtain

$$T^{\alpha\beta}=\mu(r^2\mathcal{F})^{-1}\,\delta(X)\,\delta(Y)\,\mathrm{diag}(1,0,0,-\mathcal{F}^2). \tag{45}$$

Defining the unit vector $\zeta=\partial/\partial y$ [so $\zeta^{\alpha}=(0,0,0,1)$], the pressure along the strut is $T^{\alpha\beta}\zeta_{\alpha}\zeta_{\beta}$ and the pressure on the C-metric strut is given by the integration over the X-Y plane normal to the strut,

$$p=\int dXdY\sqrt{^{(2)}g}T^{\alpha\beta}\zeta_{\alpha}\zeta_{\beta}=-\mu. \tag{46}$$

So, the pressure and mass density of the C-metric strut satisfy the relation $p=-\mu$. Since μ is negative, at both ends of the strut, one has a positive pressure pushing away the two black holes.

Alternatively, instead of Eq. (12), we could have chosen for κ the value $\kappa^{-1}=(1/2)|d_x\mathcal{G}|_{x_n}$. By doing so, we would avoid the deficit angle at the north pole ($\delta_n=0$) and leave a conical singularity at the south pole ($\delta_s>0$). This option would lead to the presence of a semi-infinite string extending from each of the black holes towards infinity along the south pole direction, which would furnish the acceleration. The mass density of both strings is $\mu=(1/4)(1-|d_x\mathcal{G}|^{-1}_{x_n}|d_x\mathcal{G}|_{x_s})>0$ and the pressure on the string, $p=-\mu$, is negative, which means that each string is pulling the corresponding black hole towards infinity.

At this point, a remark is relevant. Israel and Khan [32] have found a solution that represents two (or more) collinear Schwarzschild black holes interacting with each other in such a way that allows dynamical equilibrium. In this solution, the two black holes are connected by a strut that exerts an outward pressure which cancels the inward gravitational attraction and so the distance between the two black holes remains fixed [32]. The solution [32] is valid for $\Lambda=0$ but, although it has not been done, it can be extended in principle for generic Λ and so the present remark holds for generic Λ. Now, the C-metric solution reduces to a single nonaccelerated black hole free of struts or strings when the acceleration parameter A vanishes (see the Appendix and Sec. IV C). Thus, when we take the limit $A=0$, the C metric does not reduce to the static solution of Israel and Khan. The reason for this behavior can be found in the Carter-Penrose diagrams of the C metric. For example, looking at Fig. 4(c), which represents the massive uncharged C metric along the equator, we conclude that a null ray sent from the vicinity of one of the black holes can never cross the acceleration horizon (r_A) into the other black hole. So, if the two black holes cannot communicate through a null ray, they cannot interact gravitationally. The only interaction that is present in the system is between the strut and each one of the black holes that suffer an acceleration, which is only furnished by the strut's pressure. That the limit $A=0$ does not yield the solution [32] can also be inferred from [9], where the C metric is obtained from the two black hole solution of [32] but through a singular limit in which several quantities go appropriately to infinity.

Ernst [4] has employed a Harrison-type transformation to the $\Lambda=0$ charged C metric in order to append a suitably chosen external electromagnetic field. With this procedure, the so called Ernst solution is free of conical singularities at both poles and the acceleration that drives away the two oppositely charged Reissner-Nordström black holes is totally provided by the external electromagnetic field. In the AdS background, we cannot remove the conical singularities through the application of the Harrison transformation [33]. Indeed, the Harrison transformation does not leave invariant the cosmological term in the action. Therefore, applying the Harrison transformation to Eqs. (3)–(5) does not yield a new solution of the Einstein-Maxwell-AdS theory.

5. Radiative properties

The C metric (either in the flat, de Sitter, or anti–de Sitter background) is an exact solution that is radiative. As noticed in [3], the gravitational radiation is present since the complex scalar of the Newman-Penrose formalism, $\Psi^4=-C_{\mu\nu\alpha\beta}n^{\mu}\bar{m}^{\nu}n^{\alpha}\bar{m}^{\beta}$ (where $C_{\mu\nu\alpha\beta}$ is the Weyl tensor and $\{l,n,m,\bar{m}\}$ is the usual null tetrad of Newman-Penrose), contains a term proportional to r^{-1}. Similarly, the charged version of the C metric includes, in addition, electromagnetic radiation. In [6], it has been shown that the Bondi news functions of the flat C metric are indeed nonzero. These Bondi news functions appear in the context of the Bondi method introduced to study gravitational radiative systems. They are needed to determine the evolution of the radiative gravitational field since they carry the information concerning the changes of the system. When at least one of them is not zero, the total Bondi mass of the system decreases due to the emission of gravitational waves. The Bondi news functions of the flat C metric have been explicitly calculated in [14,15]. For a detailed review on the radiative properties of the C metric and other exact solutions, see [15]. In AdS background, these calculations have not been carried yet. Indeed, AdS still lacks a peeling theorem.

B. $A=1/\ell$: Single accelerated black hole

When $A=1/\ell$, the AdS C metric describes a single accelerated black hole. The absence of a second black hole is clearly indicated by the Carter-Penrose diagrams of Figs. 8 and 9.

This case has been studied in detail in [22], where the Randall-Sundrum model in a lower dimensional scenario was analyzed. In this scenario, the brane-world is a 2-brane moving in a 4D asymptotically AdS background. They have shown that the AdS C metric with $A=1/\ell$ describes a black hole bound to the Minkowski 2-brane. The brane tension is fine-tuned relative to the cosmological background acceleration and thus $A=1/\ell$ is precisely the acceleration that the black hole has to have in order to comove with the 2-brane. They concluded that the AdS C metric describes the final state of gravitational collapse on the brane-world. The causal structure of the massive uncharged solution (Fig. 8) has been first discussed in [22]. For completeness, we have also presented the causal diagrams of the massless uncharged solution in Fig. 7 and of the nonextremal, extremal, and naked massive charged solutions in Fig. 9.

In [22], the coordinate transformation that takes the massless uncharged AdS C metric with $A=1/\ell$ into the known description of the AdS spacetime in Poincaré coordinates is

given. From there one can easily go to the 5D description on the AdS hyperboloid. This 5D description can also be understood directly from the limits on the solutions $A>1/\ell$ and $A<1/\ell$ when $A\to 1/\ell$. Indeed, if we take the limit $A\to 1/\ell$ in Sec. IV A 2 (where we have studied the 5D description of case $A>1/\ell$), one sees that the cut that generates the two hyperbolic lines degenerates into two half circles which, on identifying the ends of the AdS hyperboloid at both infinities, yields one full circle. This means that the trajectory of the origin of the AdS C metric in the $A=1/\ell$ case is a circle (which when one unwraps the hyperboloid to its universal cover yields a straight accelerated line). As we will see in the next subsection, for $A<1/\ell$ the trajectory of the origin is a circle which, on taking the limit $A\to 1/\ell$, still yields a circle. The two limits give the same result, as expected.

C. $A<1/\ell$: Single accelerated black hole

The $A<1/\ell$ case was first analyzed in [23]. We have complemented this work with the analysis of the causal structure. The causal diagrams of this spacetime are identical to those of the AdS ($m=0$, $q=0$) [see Fig. 7(a)], of the AdS-Schwarzschild ($m>0$, $q=0$) [see Fig. 8(a)], and of the AdS–Reissner-Nordström solutions ($m>0$, $q\neq 0$) [see Fig. 9(a)]. However, the curvature singularity of the single black hole of the solution is not at rest but is being accelerated, with the acceleration A provided by an open string that extends from the pole into asymptotic infinity.

As was done with the $A>1/\ell$ case, it is useful to interpret the solution following two complementary descriptions, the 4D one and the 5D one. One first recovers the massless uncharged AdS C metric defined by Eq. (3) and Eq. (4) (with $A<1/\ell$, $m=0$, and $q=0$), and after performing the following coordinate transformation [23]:

$$T=\frac{\sqrt{1-\ell^2A^2}}{A}t,\quad R=\frac{\sqrt{1-\ell^2A^2}}{A}\frac{1}{y},$$

$$\theta=\arccos x,\quad \phi=z, \tag{47}$$

we can rewrite the massless uncharged AdS C metric as

$$ds^2=\frac{1}{\eta^2}\left[-(1+R^2/\ell^2)dT^2+\frac{dR^2}{1+R^2/\ell^2}+R^2d\Omega^2\right], \tag{48}$$

with $\eta^{-1}=\sqrt{1-\ell^2A^2}+AR\cos\theta$ and $d\Omega^2=d\theta^2+\sin^2\theta d\phi^2$. A procedure similar to the one used to obtain Eq. (35) indicates that an observer describing 4D timelike worldlines with $R=$const, $\theta=0$, and $\phi=0$ suffers a 4-acceleration with magnitude given by

$$|a_4|=\frac{\ell^2A-R\sqrt{1-\ell^2A^2}}{\ell\sqrt{\ell^2+R^2}}. \tag{49}$$

Therefore, the origin of the AdS C metric, $R=0$, is being accelerated with a constant acceleration whose value is precisely given by A. The causal diagram of this spacetime is drawn in Fig. 14. Notice that when we set $A=0$, Eq. (48) reduces to the usual AdS spacetime written in static coordinates. Now, to obtain the 5D description, one applies to Eq. (48) the coordinate transformation [23],

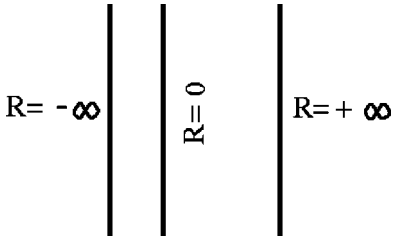

FIG. 14. Carter-Penrose diagram of metric (48).

$$z^0=\eta^{-1}\sqrt{\ell^2+R^2}\sin(T/\ell),$$

$$z^2=\eta^{-1}R\sin\theta\cos\phi,$$

$$z^4=\eta^{-1}\sqrt{\ell^2+R^2}\cos(T/\ell),$$

$$z^3=\eta^{-1}R\sin\theta\sin\phi,$$

$$z^1=\eta^{-1}[\sqrt{1-\ell^2A^2}R\cos\theta-\ell^2A]. \tag{50}$$

Transformations (50) define an embedding of the massless uncharged AdS C metric with $A<1/\ell$ into the 5D description of the AdS spacetime since they satisfy Eq. (36) and take directly Eq. (48) into Eq. (37).

The origin of the radial coordinate, $R=0$, moves in the 5D Minkowski embedding spacetime according to [see Eq. (50)]

$$z^1=-\ell^2A/\sqrt{1-\ell^2A^2},\quad z^2=0,\quad z^3=0,$$

and

$$(z^0)^2+(z^4)^2=(1/\ell^2-A^2)^{-1}\equiv a_5^{-2}. \tag{51}$$

So, contrary to the case $A>1/\ell$, where the origin described a Rindler-like hyperbolic trajectory [see Eq. (39)] that suggests the presence of two black holes driving away from each other in the extended diagram, in the $A<1/\ell$ case the origin describes a circle (a uniformly accelerated worldline) in the 5D embedding space (see Fig. 15), indicating the presence of a single trapped black hole in the AdS background.

To summarize and conclude, we present the global description on the AdS hyperboloid of the AdS C metric origin when the acceleration A varies from $+\infty$ to zero. When $A=+\infty$, the origin of the solution is represented in the hyperboloid by two mutual perpendicular straight null lines at 45° that result from the intersection of the hyperboloid surface defined by Eq. (36) and the $z^4=\ell$ plane (see Figs. 12 and 13). When A belongs to $]1/\ell,+\infty[$, the origin of the solution is represented by two hyperbolic lines [Eq. (39)] lying on the AdS hyperboloid and results from the intersection of Eq. (36) and the $z^4=\text{const}>\ell$ plane (see Fig. 12). As the acceleration approaches the value $A=1/\ell$, the separation between the two hyperbolic lines increases. When $A=1/\ell$, the separation between the two hyperbolic lines becomes infinite and they collapse into two half circles which, on identifying the

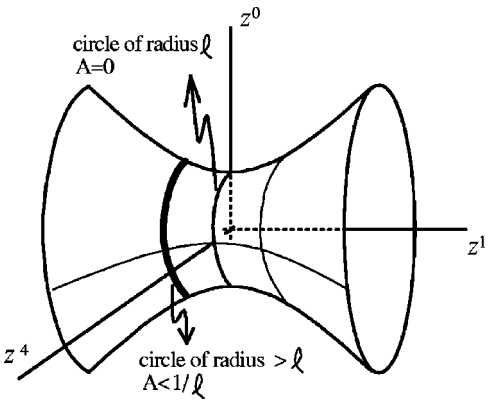

FIG. 15. AdS 4-hyperboloid embedded in the 5D Minkowski spacetime. The origin of the AdS C metric with $A<1/\ell$ moves in the hyperboloid along the circle with $z^1=\text{const}<0$. When $A=0$ this circle is at the plane $z^1=0$ and has a radius ℓ.

ends of the AdS hyperboloid at both infinities, yield one full circle in the z^0-z^4 plane at infinite z^1. At this point we see again that the value $A=1/\ell$ sets a transition stage between $A>1/\ell$ and $A<1/\ell$. When A belongs to $]0,1/\ell[$, the origin of the solution is described again by a circle [Eq. (51)] in the z^0-z^4 plane but now at a constant $z^1<0$. As the acceleration approaches the value $A=0$, the radius of this circle decreases and when $A=0$, the circle has a radius with value ℓ and is at $z^1=0$ (see Fig. 15) and we recover the usual AdS solution whose origin is at rest.

V. CONCLUSIONS

The AdS C metric found by Plebański and Demiański [16] is characterized by a quite interesting new feature when compared with the C metric in flat or de Sitter backgrounds. Indeed, contrary to what happens in these two last solutions, in the AdS background the solution only describes a pair of accelerated black holes if the acceleration parameter satisfies $A>1/\ell$, where ℓ is the cosmological length. The acceleration is caused by a strut that connects the black holes. The physical interpretation of the solutions has been essentially taken from the analysis of the Carter-Penrose diagrams (following the approach of Kinnersly and Walker [3] for the flat C metric), from the embedding of the massless uncharged solution into the AdS 4-hyperboloid in a 5D Minkowski spacetime (with two timelike coordinates), and from the physics of the strut. The alternative approach of Bonnor [7], which puts the flat C metric into the Weyl form, cannot be realized here, since the introduction of the cosmological constant prevents such a coordinate transformation.

For $A>1/\ell$, the embedding of the AdS C metric into 5D Minkowski space clearly shows that the origin of the AdS C-metric solution is subjected to a uniform acceleration, and describes a hyperbolic Rindler-like worldline in the AdS 4-hyperboloid embedded in the 5D Minkowski space. To be more precise, the origin is represented by two hyperbolic lines that approach asymptotically the Rindler-like accelerated horizon, so called because it is absent when $A=0$ and present even when $A\neq 0$, $m=0$, and $q=0$. When we add a mass or a charge to the system, the causal diagrams indicate that now we have two AdS-Schwarzschild or two AdS–Reissner-Nordström black holes approaching asymptotically the Rindler-like accelerated horizon. We have proceeded to the localization of the conical singularity present in the solution and concluded that it is between the two black holes and along the symmetry axis (or alternatively from the black holes out to infinity). When it is between the two black holes, it is associated to a strut satisfying the relation $p=-\mu>0$, where p and μ are, respectively, the pressure on the strut and its mass density. The pressure is positive, so it points outwards into infinity and pulls the black holes apart, furnishing their acceleration (as in the flat C metric). When the conical singularity points from each of the black holes into infinity, it is associated to a string with negative pressure that pushes the black holes into infinity. From the analysis of the Carter-Penrose diagrams, we also concluded that the two black holes cannot interact gravitationally. So, their acceleration is provided only by the pressure exerted by the strut. This is the reason why the limit $A=0$ of the C metric does not reduce to the static solution of Israel and Khan [32]. This solution describes two collinear Schwarzschild black holes connected by a strut that exerts an outward pressure which cancels the inward gravitational attraction and so the distance between the two black holes remains fixed.

For $A\leqslant 1/\ell$, the above procedure indicates the absence of a second black hole and so the solution describes a single black hole. In the AdS 4-hyperboloid, the origin of these solutions describes a circle in the plane defined by the two timelike coordinates. In a lower dimensional Randall-Sundrum model, it has been shown that the $A=1/\ell$ AdS C metric describes a black hole bound to a Minkowski 2-brane moving in a 4D asymptotically AdS background [22].

The C metric solution for generic Λ has been used [17,25,26] to describe the final state of the quantum process of pair creation of black holes that once created, accelerate apart by an external field. In this context, we expect that the black hole pair created in the AdS background must have an acceleration $A>1/\ell$. Indeed, the AdS background is globally contracting with an acceleration precisely equal to $1/\ell$. Therefore, a pair of virtual black holes created in this background can only become real if the black hole acceleration is greater than the contracting acceleration of the AdS background, otherwise the annihilation is inevitable. The quantum process that might create the pair would be the gravitational analogue of the Schwinger pair production of charged particles in an external electromagnetic field. This would be one possible scenario to create two exactly equal black holes with the same acceleration that are described by the AdS C-metric solution with $A>1/\ell$.

ACKNOWLEDGMENT

This work was partially funded by Fundação para a Ciência e Tecnologia (FCT) through project CERN/FIS/43797/2001 and PESO/PRO/2000/4014. OJCD also acknowledges financial support from the portuguese FCT through PRAXIS XXI program. J.P.S.L. thanks Observatório Nacional do Rio de Janeiro for hospitality.

APPENDIX: MASS AND CHARGE PARAMETERS

In this appendix, one gives the physical interpretation of parameters m and q that appear in the AdS C metric. We follow [23].

Applying the coordinate transformations to Eq. (3) (see [23]),

$$T=\sqrt{1-\ell^2A^2}A^{-1}t, \quad R=\sqrt{1-\ell^2A^2}(Ay)^{-1},$$

$$\theta=\int_x^{x_n}\mathcal{G}^{-1/2}dx, \quad \phi=z/\kappa, \tag{A1}$$

and setting $A=0$ (and $\kappa=1$) one obtains

$$ds^2=-F(R)dT^2+F^{-1}(R)dR^2 + R^2(d\theta^2+\sin^2\theta d\phi^2), \tag{A2}$$

where $F(R)=1+R^2/\ell^2-2m/R+q^2/R^2$. So, when the acceleration parameter vanishes, the AdS C metric, Eq. (3), reduces to the AdS-Schwarzschild and AdS–Reissner-Nordström black holes and the parameters m and q that are present in the AdS C metric are precisely the ADM mass and ADM electromagnetic charge of these nonaccelerated black holes. It should, however, be emphasized that the accelerated black holes lose mass through radiative processes and so the determination of the mass of the accelerated black holes would require the calculation of the Bondi mass, which we do not do here.

[1] D. Kramer, H. Stephani, M. MacCallum, and E. Herlt, *Exact Solutions of Einstein's Field Equations* (Cambridge University Press, Cambridge, England, 1980).
[2] J. Ehlers and W. Kundt, in *Gravitation: An Introduction to Current Research*, edited by L. Witten (Wiley, New York, 1962).
[3] W. Kinnersley and M. Walker, Phys. Rev. D **2**, 1359 (1970).
[4] F. J. Ernst, J. Math. Phys. **17**, 515 (1976).
[5] H. Farhoosh and R. L. Zimmerman, J. Math. Phys. **20**, 2272 (1979); Phys. Rev. D **21**, 317 (1980); **23**, 299 (1981).
[6] A. Ashtekar and T. Dray, Commun. Phys. (London) **79**, 581 (1981).
[7] W. B. Bonnor, Gen. Relativ. Gravit. **15**, 535 (1983); **16**, 269 (1984).
[8] F. H. J. Cornish and W. J. Uttley, Gen. Relativ. Gravit. **27**, 439 (1995); **27**, 735 (1995).
[9] W. Yongcheng, Phys. Rev. D **55**, 7977 (1997).
[10] C. G. Wells, ''Extending the black hole uniqueness theorems I. Accelerating black holes: The Ernst solution and C metric,'' gr-qc/9808044.
[11] V. Pravda and A. Pravdova, Class. Quantum Grav. **18**, 1205 (2001).
[12] J. Podolský and J. B. Griffiths, Gen. Relativ. Gravit. **33**, 59 (2001).
[13] J. Bičák and B. G. Schmidt, Phys. Rev. D **40**, 1827 (1989).
[14] J. Bičák, Proc. R. Soc. London **A302**, 201 (1968).
[15] V. Pravda and A. Pravdova, Czech. J. Phys. **50**, 333 (2000).
[16] J. F. Plebański and M. Demiański, Ann. Phys. (N.Y.) **98**, 98 (1976).
[17] H. F. Dowker, J. P. Gauntlett, D. A. Kastor, and J. Traschen, Phys. Rev. D **49**, 2909 (1994).
[18] H. Farhoosh and R. L. Zimmerman, Phys. Rev. D **21**, 2064 (1980).
[19] P. S. Letelier and S. R. Oliveira, Phys. Rev. D **64**, 064005 (2001).
[20] J. Bičák and V. Pravda, Phys. Rev. D **60**, 044004 (1999).
[21] J. Podolský and J. B. Griffiths, Phys. Rev. D **63**, 024006 (2001).
[22] R. Emparan, G. T. Horowitz, and R. C. Myers, J. High Energy Phys. **01**, 007 (2000); **01**, 021 (2000).
[23] J. Podolský, Czech. J. Phys. **52**, 1 (2002).
[24] A. Chamblin, Class. Quantum Grav. **18**, L17 (2001).
[25] S. W. Hawking, G. T. Horowitz, and S. F. Ross, Phys. Rev. D **51**, 4302 (1995).
[26] R. B. Mann, Class. Quantum Grav. **14**, L109 (1997); Nucl. Phys. **B516,** 357 (1998).
[27] O. J. C. Dias, in *Astronomy and Astrophysics: Recent Developments*, edited by J. P. S. Lemos *et al.* (World Scientific, Singapore, 2001).
[28] J. P. S. Lemos, Phys. Rev. D **54**, 6206 (1996).
[29] S. Deser and O. Levin, Class. Quantum Grav. **14**, L163 (1997).
[30] A. Vilenkin, Phys. Rep. **121**, 263 (1985).
[31] O. J. C. Dias and J. P. S. Lemos, Class. Quantum Grav. **19**, 2265 (2002).
[32] W. Israel and K. A. Khan, Nuovo Cimento **33**, 331 (1964); M. S. Costa and M. J. Perry, Nucl. Phys. **B591**, 469 (2000).
[33] R. Emparan (private communication).